Biallelic Variants in TONSL Cause SPONASTRIME Dysplasia and a Spectrum of Skeletal Dysplasia Phenotypes

Burrage, Lindsay; Reynolds, John; Baratang, Nissan ; Phillips, Jennifer ; Wegner, Jeremy ; McFarquhar, Ashley ; Higgs, Martin; Christiansen, Audrey ; Lanza, Denise ; Seavitt, John ; Jain, Mahim ; Li, Xiaohui ; Parry, David ; Raman, Vandana ; Chitayat, David ; Chinn, Ivan; Bertuch, Alison; Karaviti, Lefkothea ; Schlesinger, Alan ; Earl, Dawn

DOI:
10.1016/j.ajhg.2019.01.007

Biallelic Variants in *TONSL* Cause SPONASTRIME Dysplasia and a Spectrum of Skeletal Dysplasia Phenotypes

Lindsay C. Burrage,[1,2,38] John J. Reynolds,[3,38] Nissan Vida Baratang,[4] Jennifer B. Phillips,[5] Jeremy Wegner,[5] Ashley McFarquhar,[4] Martin R. Higgs,[3] Audrey E. Christiansen,[6] Denise G. Lanza,[1] John R. Seavitt,[1] Mahim Jain,[7] Xiaohui Li,[1] David Parry,[8] Vandana Raman,[9] David Chitayat,[10,11] Ivan K. Chinn,[12,13] Alison A. Bertuch,[1] Lefkothea Karaviti,[14] Alan E. Schlesinger,[15] Dawn Earl,[16] Michael Bamshad,[16,17] Ravi Savarirayan,[18] Harsha Doddapaneni,[19] Donna Muzny,[19] Shalini N. Jhangiani,[19] Christine Eng,[1,20] Richard A. Gibbs,[1,19] Weimin Bi,[1,20] Lisa Emrick,[1,12,21] Jill A. Rosenfeld,[1] John Postlethwait,[5] Monte Westerfield,[5] Mary E. Dickinson,[1,6] Arthur L. Beaudet,[1] Emmanuelle Ranza,[22] Celine Huber,[23] Valérie Cormier-Daire,[23] Wei Shen,[24, 25] Rong Mao,[24,25] Jason D. Heaney,[1] Jordan S. Orange,[13,26] University of Washington Center for Mendelian Genomics, Undiagnosed Diseases Network, Débora Bertola,[27,28] Guilherme Yamamoto,[27,28] Wagner A.R. Baratela,[27] Merlin G. Butler,[29] Asim Ali,[30] Mehdi Adeli,[31] Daniel H. Cohn,[32] Deborah Krakow,[33] Andrew P. Jackson,[34] Melissa Lees,[35] Amaka C. Offiah,[36] Colleen M. Carlston,[25] John C. Carey,[37] Grant S. Stewart,[3,39] Carlos A. Bacino,[1,2,39] Philippe M. Campeau,[4,39] Brendan Lee[1,2,39*]

1. Department of Molecular and Human Genetics, Baylor College of Medicine, Houston, TX 77030, USA
2. Texas Children's Hospital, Houston, TX 77030, USA
3. Institute of Cancer and Genomic Sciences, University of Birmingham, Birmingham B15 2TT, UK
4. CHU Sainte-Justine Research Center, University of Montreal, Montreal, QC H3T1J4, Canada
5. Institute of Neuroscience, University of Oregon, Eugene, OR 97403, USA
6. Department of Molecular Physiology and Biophysics, Baylor College of Medicine, Houston, TX 77030, USA
7. Department of Bone and OI, Kennedy Krieger Institute, Baltimore, MD 21205, USA
8. MRC Institute of Genetics & Molecular Medicine, The University of Edinburgh, Western General Hospital, Crewe Road, Edinburgh EH4 2XU, UK
9. Division of Pediatric Endocrinology and Diabetes, University of Utah, Salt Lake City, UT 84112, USA
10. The Prenatal Diagnosis and Medical Genetics Program, Department of Obstetrics and Gynecology, Mount Sinai Hospital, University of Toronto, Toronto, Ontario M5G 1Z5, Canada
11. Department of Pediatrics, Division of Clinical and Metabolic Genetics, the Hospital for Sick Children, University of Toronto, Toronto, ON M5G 1X8, Canada
12. Department of Pediatrics, Baylor College of Medicine, Houston, TX 77030, USA
13. Division of Pediatric Immunology, Allergy, and Rheumatology, Texas Children's Hospital, Houston, TX 77030, USA
14. Division of Diabetes and Endocrinology, Texas Children's Hospital, Houston, TX 77030, USA

15. Department of Pediatric Radiology, Texas Children's Hospital; Department of Radiology, Baylor College of Medicine, Houston, TX 77030, USA
16. Seattle Children's Hospital, Seattle, WA 98195, USA
17. Departments of Pediatrics and Genome Sciences, University of Washington, Seattle, WA 98195, USA
18. Victorian Clinical Genetics Services, Murdoch Children's Research Institute, University of Melbourne, Parkville, Victoria 3052, Australia
19. Human Genome Sequencing Center, Baylor College of Medicine, Houston, TX 77030, USA
20. Baylor Genetics, Houston, TX 77030, USA
21. Division of Neurology and Developmental Neuroscience and Department of Pediatrics, Baylor College of Medicine, Houston, TX 77030, USA
22. Service of Genetic Medicine, University of Geneva Medical School, Geneva University Hospitals, 1205 Geneva, Switzerland
23. Department of Genetics, INSERM UMR1163, Université Paris Descartes-Sorbonne Paris Cité, Institut Imagine, AP-HP, Hôpital Necker Enfants Malades, Paris 75015, France
24. ARUP Laboratories, Salt Lake City, UT 84108, USA
25. Department of Pathology, University of Utah, Salt Lake City, UT 84112, USA
26. Current affiliation: Department of Pediatrics, Columbia University Vagelos College of Physicians and Surgeons, New York Presbyterian, New York, NY 10032, USA
27. Clinical Genetics Unit, Instituto da Criança, Hospital das Clínicas da Faculdade de Medicina da Universidade de São Paulo, São Paulo SP 05403-000, Brazil
28. Centro de Pesquisa sobre o Genoma Humano e Células-Tronco, Instituto de Biociências da Universidade de São Paulo, SP, 05508-0900, Brazil
29. Departments of Psychiatry & Behavioral Sciences and Pediatrics, Kansas University Medical Center, Kansas City, KS, USA, 66160.
30. Department of Ophthalmology & Vision Sciences, Hospital for Sick Children and University of Toronto, Toronto, Ontario M5G 1X8, Canada
31. Department of Allergy and Immunology, Sidra Medicine / Hamad Medical Corporation / Weill Cornell Medicine - Qatar, Doha, Qatar
32. Department of Molecular, Cell, and Developmental Biology and Department of Orthopaedic Surgery, University of California, Los Angeles, Los Angeles, CA 90095, USA
33. Department of Orthopaedic Surgery, Department of Human Genetics and Department of Obstetrics and Gynecology, David Geffen School of Medicine at UCLA, University of California, Los Angeles, Los Angeles, CA 90095, USA
34. MRC Human Genetics Unit, Institute of Genetics and Molecular Medicine, University of Edinburgh, Edinburgh EH4 2XU, UK
35. North East Thames Regional Genetics Service, Great Ormond Street Hospital, London WC1N 3JH, UK
36. Department of Oncology and Metabolism, Academic Unit of Child Health, University of Sheffield, Sheffield S10 2TH, UK
37. Department of Pediatrics, Division of Medical Genetics, University of Utah, Salt Lake City, UT 84112, USA
38. These authors contributed equally to this work.

39. These authors contributed equally to this work.

*Corresponding Author:
Brendan Lee, M.D., Ph.D.
Department of Molecular and Human Genetics
Baylor College of Medicine
One Baylor Plaza, BCM 225
Houston, TX 77030
Email address: blee@bcm.edu

Abstract

SPONASTRIME dysplasia is an autosomal recessive spondyloepimetaphyseal dysplasia characterized by spine abnormalities (spondylar), midface hypoplasia with a depressed nasal bridge, metaphyseal striations, and disproportionate short stature. Scoliosis, coxa vara, childhood cataracts, short dental roots, and hypogammaglobulinemia have also been reported in this disorder. Although an autosomal recessive inheritance pattern has been hypothesized, pathogenic variants in a specific gene have not been discovered in individuals with SPONASTRIME dysplasia. Here, we identified biallelic variants in *TONSL*, which encodes the Tonsoku-like DNA repair protein, in nine individuals from eight families with SPONASTRIME dysplasia, and four subjects from three families with short stature of varied severity and spondylometaphyseal dysplasia with or without immunologic and hematologic abnormalities but no definitive metaphyseal striations at diagnosis. The finding of early embryonic lethality in a *Tonsl*$^{-/-}$ murine model, and the discovery of reduced length, spinal abnormalities, reduced numbers of neutrophils and early lethality in a *tonsl*$^{-/-}$ zebrafish model, support the hypomorphic nature of the identified *TONSL* variants. Moreover, functional studies revealed increased levels of spontaneous replication fork stalling and chromosomal aberrations and fewer camptothecin (CPT)-induced RAD51 foci in subject-derived cell lines. Importantly, these cellular defects were rescued upon re-expression of wild type *TONSL*, consistent with the hypomorphic *TONSL* variants being pathogenic. Overall, our studies in humans, mouse, zebrafish, and subject-derived cell lines confirm that pathogenic variants in *TONSL* impair DNA replication and

homologous recombination-dependent repair processes and lead to a spectrum of skeletal dysplasia phenotypes with numerous extra-skeletal manifestations.

Introduction

SPONASTRIME dysplasia (MIM: 271510) is an autosomal recessive spondyloepimetaphyseal dysplasia named for characteristic clinical and radiographic findings including spine abnormalities (spondylar), midface hypoplasia with a depressed nasal bridge, and striation of the metaphyses [1]. Additional features include disproportionate short stature with exaggerated lumbar lordosis, scoliosis, coxa vara, limited elbow extension, childhood cataracts, short dental roots, and hypogammaglobulinemia [2-9]. Radiographically, the abnormalities of the lumbar vertebral bodies are suggested to be the most specific finding because the characteristic metaphyseal striations may not be apparent at young ages [10]. Multiple affected siblings have been reported with SPONASTRIME dysplasia [1; 2; 6], and thus, an autosomal recessive inheritance pattern has been suspected. However, no gene has been associated with this disorder.

To identify a genetic basis for SPONASTRIME dysplasia, we performed whole exome sequencing and identified variants in *TONSL* (MIM: 604546) in individuals with this diagnosis and in individuals with other skeletal dysplasia phenotypes. We used studies in knockout mouse and zebrafish models and functional studies in subject-derived fibroblasts to demonstrate the essential nature of TONSL and show that reduced TONSL function is associated with replication fork and chromosomal instability, which likely contributes to the phenotypes observed in individuals with biallelic *TONSL* variants.

Materials and Methods

Human subjects and sequencing studies. Informed consent for all subjects (except subject 11) was obtained in accordance with research protocols that were approved by the Institutional Review Board at Baylor College of Medicine (BCM), the National Institutes of Health, or at local institutions prior to testing. Sample for subject 11 was obtained from the Biobank, and consent was obtained as per the protocol for Biobank submission [11]. For subjects 2, 3-1, 4, 7-1, and 7-2, informed consent for publication of photographs was obtained.

DNA was extracted from peripheral blood mononuclear cells for exome sequencing. For families 1, 2, 9 and 11, exome sequencing was performed at the Human Genome Sequencing Center (HGSC) at Baylor College of Medicine. Using 1 ug of DNA an Illumina paired-end pre-capture library was constructed according to the manufacturer's protocol (Illumina Multiplexing_SamplePrep_Guide_1005361_D) with modifications as described in the BCM-HGSC Illumina Barcoded Paired-End Capture Library Preparation protocol. Pre-capture libraries were pooled into 4-plex library pools and then hybridized in solution to the HGSC-designed Core capture reagent [12] (52Mb, NimbleGen) or 6-plex library pools used the custom VCRome 2.1 capture reagent1 (42Mb, NimbleGen) according to the manufacturer's protocol (NimbleGen SeqCap EZ Exome Library SR User's Guide) with minor revisions. The sequencing run was performed in paired-end mode using the Illumina HiSeq 2000 platform, with sequencing-by-synthesis reactions extended for 101 cycles from each end and an additional 7 cycles for the index read. With a sequencing yield of 10.6 Gb, the sample achieved 91% of the targeted exome bases covered to a depth of 20X or greater. Illumina sequence analysis was performed using the HGSC Mercury analysis pipeline [13; 14] which moves data through

various analysis tools from the initial sequence generation on the instrument to annotated variant calls (SNPs and intra-read in/dels). For subject 3-1, trio exome sequencing was performed at ARUP Laboratories using Illumina SureSelect XT kit reagents and a HiSeq2500 platform (Illumina, San Diego, CA), and the identified variants in *TONSL* were confirmed in subject 3-2 using Sanger sequencing. For family 5, exome capture was performed at the genomic platform of the IMAGINE Institute (Paris, France) with the SureSelect Human All Exon kit (Agilent Technologies). Agilent SureSelect Human All Exon (V4) libraries were prepared from 3 µg of genomic DNA sheared with Ultrasonicator (Covaris) as recommended by the manufacturer. Barcoded exome libraries were pooled and sequenced using HiSep2500 (Illumina) generating paired-end reads. After demultiplexing, sequences were mapped on the human genome reference (NCBI build37/hg 19 version) with BWA [15]. The mean depth of coverage obtained for each sample was ≥ x80 with 95% of the exome covered at least x15. Variant calling was carried out with the Genome Analysis Toolkit (GATK) [16], SAMtools [17] and Picard Tools. Single nucleotide variants were called with GATK Unified Genotyper, whereas indel calls were made with the GATK IndelGenotyper_v2. All variants with a read coverage ≤x2 and a Phred-scaled quality of ≤20 were filtered out. All the variants were annotated and filtered using an in-house developed annotation software system (Polyweb, unpublished). We first focused our analyses on non-synonymous variants, splice variants, and coding indels. The potential pathogenicity of variants was evaluated using SIFT [18] (cutoff ≤0.05), PolyPhen2 [19] (HumVar scores, cutoff ≥0.447) and Mutation Taster [20] (cutoff: qualitative prediction as pathogenic) prediction algorithms. We also assessed frequency in control populations and datasets including the ExAC database, dbSNP129, the 1000 Genomes

project, ClinVar, HGMD and in-house exome data. All variants (except the variants in subject 14) were confirmed by Sanger sequencing and correct family segregation was verified. For family 6, exome sequencing was performed as described previously [21]. Family 7, which was enrolled in the Undiagnosed Diseases Network, and family 8 had exome sequencing at Baylor Genetics Laboratories, as described elsewhere[22]. Codified genomics variation interpretation software was used for variant review in families 7 and 8. Exome sequencing and analysis was performed as described previously for subject 10[23], subject 12[24], and subject 13[24]. For subject 14, exome was sequenced at CEGH-CEL-Universidade de São Paulo, the capture library was an Illumina TrueSeq kit, sequencing was done an on Illumina HiSeq, alignment with the Burrows-Wheeler Aligner (BWA), and annotation with GATK/ ANNOVAR. Sanger sequencing of the *TONSL* exons was performed in DNA from subject 4 and 15 using primers in Table S1. Sanger confirmations were performed using Big Dye® Terminator v3.1 and an ABI 3730 DNA Analyzer (Life Technologies, Carlsbad, CA). Sanger confirmation for subject 2 was performed by submission of PCR products to Genewiz (La Jolla, CA). All variants are provided using hg19, NM_013432.4.

Tonsl$^{-/-}$ *mouse generation and analysis*. Single guide RNA (sgRNA) sequences were selected to target intronic sequences flanking exons 12-18 of *Tonsl* (chr15:76,635,006-76,635,028 and chr15:76,632,468-76,632,490; GRCm38/mm10) using the Wellcome Trust Sanger Institute (WTSI) Genome Editing website [25]. DNA templates for *in vitro* transcription of sgRNAs were produced using overlapping oligonucleotides in a high-fidelity PCR reaction [26] and sgRNA was transcribed using the MEGA shortscript T7 kit

(ThermoFisher, Waltham, MA). Cas9 mRNA was purchased from ThermoFisher. Cas9 mRNA (100 ng/µl) and sgRNA (10 ng/µl) in RNase-free 1xPBS were injected into the cytoplasm of 100 pronuclear stage C57Bl/6NJ embryos. Primers P1 (5' CTTCAGCTGGTGGCCACAT), P2 (5' TCTCCCATGTCATTGCGCC), P3 (5' GCCCTCTCTAAGGCCCATAG) were used for genotyping and sequencing founder animals and subsequent generations (P1 and P2 amplify the wild-type allele; P1 and P3 amplify the null allele). All mouse studies were approved by the BCM Institutional Animal Care and Use Committee (IACUC).

tonsl$^{-/-}$ *zebrafish generation and analysis.* Zebrafish were raised according to standard protocols [27] and in accordance with University of Oregon IACUC protocols. Oregon AB* and *Tg(mpx:GFP)*^{i114} lines were used [28] . The zebrafish-Codon-Optimized Cas9 plasmid [29] that was digested with *Xba*I, purified and transcribed using T3 message machine kit (Ambion, Austin, USA). gRNA was designed (using the ZiFiT Targeter software) to the CRISPR target sequence GGAGAGTGCTATGCAGAGCT at the 3' end of *tonsl* exon 3. Templates for gRNA synthesis were prepared by PCR using the gene-specific primer: 5`-AATTAATACGACTCACTATA-[20 bp Target Sequence]-GTTTTAGAGCTAGAAATAGC-3` and the gRNA scaffold primer: 5`-GATCCGCACCGACTCGGTGCCACTTTTTCAAGTTGATAACGGACTAGCCTTATTTT AACTTGCTATTTCTAGCTCTAAAAC-3` using an annealing temperature of 60°C. sgRNA was synthesized using T7 Megascript kit, (Ambion, Austin, USA). Cas9 mRNA (300 ng/µl) and sgRNA (150 ng/µl) were mixed and injected into Oregon AB* wild-type zebrafish embryos at the one cell stage using an MPPI-2 Pressure Injector with a BP-15

Back Pressure Unit (Applied Scientific Instrumentation, Oregon USA). Sequence analysis of pools of injected embryos at 24 hours post fertilization (hpf) using primers Tonsl e3-6F:CCCTAGGTGACTATCAAGCTGC and Tonsl e3+129R ACATGCATGCGTTTACTGTAGC to amplify the region containing the target sequence confirmed CRISPR activity at the target site, and analysis of individual F1 embryos at 24 hpf identified clutches carrying frameshift mutations, which were then propagated and crossed to examine the recessive phenotype. Two frameshift deletions of 5 and 13 bp, respectively, affecting both alternate 5' – 3' reading frames in exon 3, were recovered in F1 progeny of injected founders. Skeletal elements were stained with Alcian Blue and Alizarin Red as previously described [30] . Images were captured using a Leica S8APO dissecting microscope fitted with a Leica EC3 camera and LAZ EZ imaging software. Statistical analyses were performed using GraphPad software.

Cell culture and generation of cell lines. Dermal primary fibroblasts were grown from skin-punch biopsies and maintained in Dulbecco's modified Eagle's medium (DMEM; Life Technologies) supplemented with 20% FCS, 5% L-glutamine and 5% penicillin-streptomycin (Invitrogen) antibiotics. Subject-derived cell lines were validated using Sanger sequencing and immunoblotting. Primary fibroblasts were immortalized with 293FT-derived supernatant containing a human telomerase reverse transcriptase (TERT) lentivirus that was generated using the plasmids: pLV-hTERT-IRES-hygro (gift from Tobias Meyer; Addgene #85140), psPax2 (gift from Didier Trono; Addgene #12260) and pMD2.G (gift from Didier Trono; Addgene #12259). Selection was performed using hygromycin (Invitrogen) at 70 µg/ml. Fibroblast complementation was carried out using a

lentiviral vector encoding Flag-tagged *TONSL* (gift from Dr. Yonghwan Kim). All cell lines were routinely tested for mycoplasma. ATLD2 is a fibroblast cell line derived from an individual with ataxia-telangiectasia-like disorder (ATLD, MIM:604391) who has biallelic pathogenic variants in *MRE11* (MIM:600814) [31].

Immunoblot analysis and antibodies. Whole-cell extracts were prepared from harvested subject-derived fibroblasts by sonication in UTB buffer (8 M urea, 50 mM Tris, 150 mM β-mercaptoethanol). Whole-cell extracts were then analyzed by SDS–PAGE on 6% acrylamide gels following standard procedures. Protein samples were transferred onto a nitrocellulose membrane, and immunoblotting was performed using antibodies to TONSL (1:200; the kind gift of D. Durocher, Toronto, Canada) [32] and DNA-PK_{CS} (Santa Cruz Biotechnology, [G-4] sc-5282; 1:2000).

Immunofluorescence and fluorescence microscopy. Subject-derived fibroblasts were seeded onto coverslips at least 48 h before extraction and fixation. Cells were pre-extracted for 5 min on ice with ice-cold buffer (25 mM HEPES, pH 7.4, 50 mM NaCl, 1 mM EDTA, 3 mM MgCl2, 300 mM sucrose and 0.5% Triton X-100) and then fixed with 4% paraformaldehyde for 10 min. Fixed cells were stained with primary antibodies specific to γH2AX (Millipore, 05-636; 1:1,000) and RAD51 (Merck, PC130; 1:500), with secondary antibodies conjugated to Alexa Fluor 488 and Alexa Fluor 594 (Life Technologies), and then with DAPI. Images were visualized using a Nikon Eclipse Ni microscope with NIS-Elements software (Nikon Instruments) and captured using a 100× oil-immersion objective.

DNA-fiber-spreading assay. Subject-derived fibroblasts were seeded for at least 48 h prior to harvesting. Cells were pulse-labelled with 25 μM CldU for 30 min, washed with PBS, pulse-labelled with 250 μM IdU with or without 50 nM CPT, and harvested by trypsinization. The cells were washed with PBS and resuspended to a concentration of 5 × 10^5/ml in PBS. The cells were then lysed in spreading buffer (200 mM Tris-HCl, pH 7.5, 50 mM EDTA, 0.5% SDS) directly on glass microscope slides, and DNA fibers were allowed to spread down the slide by gravity. The slides were then fixed in methanol:acetic acid (3:1 ratio), denatured with 2.5 M HCl, and CldU and IdU was detected using rat anti-BrdU antibody (clone BU1/75, ICR1; Abcam, ab6326; 1:750) and mouse anti-BrdU antibody (clone B44; BD Biosciences, 347583; 1:750). Slides were fixed in 4% paraformaldehyde before immunostaining with secondary antibodies conjugated to Alexa Fluor 594 or Alexa Fluor 488 (Life Technologies). Labelled DNA fibers were visualized using a Nikon Eclipse Ni microscope with 60× oil-immersion objectives and images were acquired using NIS-Elements software (Nikon Instruments). Replication fork structures (>1000 fork structures) and CldU/IdU track lengths (>300 ongoing forks) were then quantified using ImageJ software (US National Institutes of Health; NIH).

Metaphase spreads. Giemsa-stained metaphase spreads were prepared as previously described[21]. Briefly, Colcemid (KaryoMAX™, Life Technologies) was added at a final concentration of 0.2 μg/ml for 4 hours. Cells were then harvested by trypsinization, subjected to hypotonic shock for 30 min at 37 °C in hypotonic buffer (10mM KCl, 15% FCS) and fixed in 3:1 ethanol:acetic acid solution. Cells were dropped onto acetic-acid-

humidified slides, stained for 15 min in Giemsa-modified solution (Sigma; 5% vol/vol in water) and washed in water for 5 min.

Statistics

Statistical analysis was performed as indicated in tables and in figure legends. Significance is indicated by a p value of less than 0.05.

Results

Biallelic variants in TONSL cause a spectrum of skeletal dysplasia phenotypes

We performed exome sequencing in 10 probands with a clinical diagnosis of SPONASTRIME dysplasia who were identified by the Baylor-Texas Children's Hospital Skeletal Dysplasia Program, the International Skeletal Dysplasia Registry, GeneMatcher [33] and various collaborators who are experts in skeletal dysplasias (Table 1, Table S2 and S3). Biallelic variants in *TONSL*, which encodes the Tonsoku-like DNA repair protein, were identified in six of the ten subjects with SPONASTRIME dysplasia (Table 2). Two additional subjects (subjects 4 and 15) with SPONASTRIME dysplasia and biallelic variants in *TONSL* were identified by Sanger sequencing of the coding region of the gene (Table 1, 2, S2). In addition, subject 3-2 was confirmed to have the same variants in *TONSL* as his sibling (3-1) using Sanger sequencing. These nine subjects had significant disproportionate short stature, spine abnormalities, and characteristic facial features including midface hypoplasia with a depressed nasal bridge (Figure 1A, Figures S1, Table S2). All but the youngest subject (3-2) also had metaphyseal striations. Other features included bilateral cataracts in three subjects, subglottic stenosis in three subjects, shallow

dental roots in four subjects, and a history of hypogammaglobinemia in two subjects. Clinical information about subject 4 and 15 has been published previously [4; 7; 8]. Biallelic variants in *TONSL* or in *MMS22L* (MIM: 615614), the gene encoding the binding partner for TONSL, were not detected in the other four subjects (subjects 9 – 12) with a clinical diagnosis of SPONASTRIME dysplasia suggesting that this phenotype is genetically heterogeneous (Table S3). However, single heterozygous variants in *TONSL* were identified in subjects 9 and 10 (the p.Arg934Trp variant, which was also identified in individuals 1, 3, 14 and 15, and a splice site variant, respectively). Thus, we cannot rule out the possibility that deep intronic variants, promoter variants or large intragenic rearrangements/deletions in *TONSL* could be present in subjects 9 - 12. In the two subjects without any *TONSL* rare variants (subjects 11 and 12), exome analysis did not identify any sharing of genes with rare variants, nor did the analysis reveal any variants in genes encoding for TONSL interactors or related proteins.

Simultaneously, exome sequencing independently revealed biallelic variants in *TONSL* in three subjects (7-1, 7-2, and 8) from two families with spondylometaphyseal dysplasia and immunologic and hematologic abnormalities (hypogammaglobulinemia and neutropenia, respectively) and in subject 6 who had spondylometaphyseal dysplasia with severe short stature, primary aphakia, and absent pupils. Detailed clinical information is provided in Table 1, 3, S2, S3, S4 and Figure 1A, S1. All individuals except two (subjects 3-1 and 3-2) had a frameshift, nonsense or splice variant in combination with a missense variant in *TONSL*. All missense variants had CADD scores greater than 15 [34], and all but one of the missense variants were predicted to be damaging or probably

damaging by both SIFT and Polyphen-2 [18; 19] . The variants are provided in Table 2 and 4 and in Figure 1B. Details regarding the exome analysis are provided in Table S5.

Since all subjects except the siblings from family 3 had one frameshift, nonsense, or splice variant associated with an amino acid substitution, we hypothesized that biallelic partial loss of TONSL function may explain the phenotype in our subjects. To investigate the impact of variants identified in our subjects on TONSL protein stability, we performed immunoblot analyses on three subject-derived fibroblast cell lines that had a range of *TONSL* variants. This analysis revealed the cell line from subject P6 (p.Gln713*;p.Thr653Met) produced little to undetectable levels of full length TONSL protein (Figure 1C), perhaps reflecting the deleterious impact of the two variants on TONSL protein stability. However, since the antibody used was raised against a fragment of recombinant TONSL comprising residues 559-809, a region encompassing both mutations in P6, it cannot be ruled out that the absence of a signal may result from the loss of the epitope recognition. Interestingly, in contrast, near normal levels of TONSL protein were detected in cell lines derived from subjects P3-1 (p.Arg934Trp;p.Ser1197Pro) and P7-1 (p.Glu199Lys;c.866-1G>C) (Figure 1C), indicating that individual *TONSL* variants have a differential effect on protein stability. Of note, the anti-TONSL antibody used for Western blotting detected two major bands. While the origin of these is unclear, we hypothesize that they represent either different isoforms or that this is caused by post-translational modification of the protein.

Early lethality in mouse and zebrafish models of TONSL deficiency

To investigate the impact of TONSL deficiency on development with *in vivo* models, we identified a *Tonsl* knockout mouse that was generated by the BCM Knockout Mouse Phenotyping Program (KOMP2). Exons 12 to 18 of *Tonsl* were deleted in a knockout mouse (*Tonsl*$^{em1(IMPC)Bay}$, *Tonsl*$^{-/-}$) which was generated using CRISPR-Cas9 technology as described previously [35; 36] (Figure S3). Deletion of these exons is predicted to result in a frameshift and premature stop codon leading to nonsense mediated decay. In collaboration with KOMP2, we detected no homozygous *Tonsl*$^{-/-}$ mice at weaning (Table 5). Moreover, embryonic genotyping was performed, and no homozygous mice were detected as early as E9.5, suggesting that murine *Tonsl* deficiency causes lethality early in embryogenesis (Table 5).

To investigate the impact of TONSL deficiency on embryonic development further, we used CRISPR/Cas9 to generate early frameshift mutations in the zebrafish *tonsl* gene (Figure S4). Zebrafish *tonsl*$^{-/-}$ mutants undergo normal embryonic development and are indistinguishable from wild-type siblings up to 6 days post fertilization (dpf), but begin to show reduced fitness and delayed growth thereafter (Figure 2A-B), with 100% mortality observed before 20 dpf. Using cartilage and bone staining to examine skeletal development, we observed that ossification of vertebral bodies around the notochord was significantly accelerated in *tonsl*$^{-/-}$ larvae at 7 dpf compared to wild-type siblings (Figure 2C). Because of the clinical findings of neutropenia in a subset of individuals in this study, we crossed carriers of the truncating *tonsl* alleles into a transgenic zebrafish line in which neutrophils fluoresce from day 2 onward. We observed normal neutrophil development in *Tg(mpo:gfp;tonsl*$^{-/-}$*)* mutants through 6 dpf, followed by diminishing neutrophil numbers correlated with the progressive decline in fitness characteristic of these mutants (Figure

2D-E). Although analysis is somewhat limited by early lethality, the larval phenotypes are reminiscent of the short stature and immunologic and spinal abnormalities exhibited by individuals with pathogenic variants in *TONSL*, which progressively gets worse with age and development (Table 1, 3, S2, S4). Together, these *in vivo* models of TONSL deficiency demonstrate the essential function of the protein.

Defective formation of RAD51-induced foci in fibroblast cell lines derived from individuals with TONSL variants

TONSL is homologous to the plant DNA repair protein, Tonsuku/Brushy1/Mgoun3 and is necessary for the repair of replication-associated DNA damage in conjunction with its obligate binding partner, MMS22L [32; 37-39]. Although the TONSL-MMS22L complex is reported to bind to all replication forks, increased binding has been noted at stalled forks and sites of DNA damage [32; 37-40], where the complex promotes efficient homologous recombination (HR)-dependent repair and the restart of stalled replication forks by stimulating RAD51-ssDNA nucleofilament formation [38; 40]. As a consequence, loss of TONSL leads to increased levels of S-phase associated DNA damage, defective HR and renders cells hypersensitive to DNA damage inducing agents, such as the topoisomerase 1 inhibitor camptothecin (CPT) [32; 37-40].

Given the lethality of TONSL deficiency in murine and zebrafish models, we investigated the functional effects of *TONSL* variants using subject-derived cell lines. Fibroblast cell lines were successfully generated from three subjects and attempted in two additional subjects, but the cell lines from these two subjects failed repeatedly due to poor growth, a finding which was not unexpected given the function of TONSL during

DNA replication. Consistent with the role of TONSL in promoting RAD51 nucleofilament formation, all three subject-derived cell lines exhibited defective formation of CPT-induced RAD51 foci as measured by immunofluorescence (Figure 3A-B).

Following this, we used the DNA fiber technique to assess the impact of the *TONSL* variants on replication fork dynamics [41; 42]. This analysis revealed that all three subject-derived cell lines exhibited a significant increase in levels of spontaneously stalled replication forks, with a concurrent decrease in ongoing forks, demonstrating that defects in TONSL give rise to replication fork instability (Figure 4A and 4B). We next investigated the ability of subject-derived cell lines to replicate in the presence of CPT. To this end, we performed DNA fiber analysis with low dose CPT (50nM) co-incubated with the second label (IdU) (Figure 4A). We then measured IdU tract length (normalized to CldU tract length), as a readout of the rate of replication fork progression in the presence of CPT. Strikingly, two of the three subject-derived cell lines (P6 and P7-1) exhibited significantly reduced rates of replication fork progression in the presence of CPT (expressed as a ratio of IdU / CldU tract length) (Figure 4C), consistent with the role for TONSL in promoting DNA replication in the presence of DNA damage [37]. The P3-1 cell line did not exhibit a detectable reduction in replication fork progression upon CPT exposure. This raises the possibility that either not all of the *TONSL* variants have the same level of impact on TONSL function or that the DNA fibre assay used is not sensitive enough to detect mild defects in replication fork progression. However, these findings could, in part, explain the variation in clinical phenotypes exhibited by the individuals with *TONSL* variants.

To confirm that this observed cellular defects were due to variants in *TONSL*, we complemented two subject-derived fibroblast cell lines (P3-1 and P6) with either an empty

vector or a vector expressing Flag-tagged wild type *TONSL* using a lentiviral expression system (Figure 5A). Importantly, re-expression of wild type *TONSL* rescued CPT-induced RAD51 foci formation and reduced the spontaneous replication fork instability observed in both P3-1 and P6 fibroblast cells lines (Figure 5B-D). Furthermore, the reduced rates of replication fork progression in the presence of CPT exhibited by P6 was also corrected (Figure 5E).

Lastly, to ascertain the pathogenic impact that the increased replication fork stalling may have on genome stability, we assessed metaphase spreads from the complemented subject-derived fibroblast cell lines for increased spontaneous chromosome breakage. In keeping with the observed replication abnormalities, both subject-derived fibroblast cell lines complemented with the empty vector exhibited increased levels of spontaneous chromosomal aberrations, which was rescued upon re-expression of wild type *TONSL*. This demonstrates that the replication defects observed in subject-derived cell lines gives rise to increased genome instability (Figure 6A-B). Taken together, these data confirm at the cellular level the pathogenicity of the *TONSL* variants identified in these cell lines derived from both SPONASTRIME and non-classical TONSL individuals.

Discussion

In this study, we demonstrate that biallelic variants in *TONSL* are associated with a spectrum of skeletal dysplasia phenotypes ranging from clinical SPONASTRIME dysplasia with marked disproportionate short stature to mild short stature with immunologic and hematologic abnormalities in 13 subjects from 11 families. We also

show that several clinical features of these subjects are recapitulated by the zebrafish *tonsl* knockout model. Importantly, *TONSL* is the first gene associated with the SPONASTRIME dysplasia phenotype. In contrast, we were unable to identify variants in *TONSL* or *MMS22L* in four subjects with a clinical diagnosis of SPONASTRIME dysplasia using exome sequencing. This result suggests that SPONASTRIME dysplasia is genetically heterogeneous. An alternative hypothesis is that non-coding variants in *TONSL* could contribute to the phenotype in these subjects and that further genome sequencing studies are warranted to rule out this possibility.

One striking finding from our study is the clinical variability of disease presentation and severity caused by pathogenic variants in the same gene. While the majority of subjects with *TONSL* variants were clinically diagnosed with SPONASTRIME dysplasia or a disorder exhibiting many features consistent with SPONASTRIME dysplasia (subjects 6, 7-1, 7-2, and 8), a lack of diagnostic features, such as absent metaphyseal striations (subject 6) or short stature (subjects 7-1 and 7-2), or the presence of atypical clinical abnormalities, such as severe microcephaly and primary aphakia (subject 6), and congenital neutropenia (subjects 7-1, 7-2, and 8), were noted in some subjects. Interestingly, this phenotypic variability has also been noted in other skeletal dysplasias caused by pathogenic variants in replication/repair genes, such as *RECQL4* (MIM: 603780) and *SMARCAL1* (MIM: 606622) [43; 44]. Although the underlying cause of this clinical heterogeneity is unclear, it is likely due, at least in part, to both the severity of the individual hypomorphic variants and the impact that each hypomorphic variant has on protein stability and/or function. Notably, several of the missense variants identified in the affected individuals localize within the central portion of the TONSL protein that contains

the ankyrin-repeats, which was previously shown to be required to mediate its interaction with replisome components, its accumulation at damaged forks/DNA lesions, and its histone chaperone and epigenetic reader activity [32; 37; 38]. Furthermore, previous cell studies have demonstrated that deletions involving the ankyrin-repeats lead to defective recruitment of TONSL to sites of damaged replication forks and increased levels of replication-associated DNA damage [32; 37; 38]. This finding suggests that the abnormal growth exhibited by individuals with *TONSL* variants may result from defective cellular replication beginning during development *in utero*. Consistent with this hypothesis, most subjects in our cohort with biallelic variants in *TONSL* presented with evidence of early short stature with reduced length in the newborn period. Moreover, all of the cell lines derived from affected individuals exhibited a significant increase in spontaneous replication fork stalling, which is a phenotype that is commonly observed in cell lines derived from individuals with replication defective-associated microcephalic dwarfism (MD), such as MD-DONSON (MIM: 617604), or microcephalic primordial dwarfism (MPD), such as ATR-Seckel Syndrome (MIM: 210600) and MPD-TRAIP (MIM: 605958) [21; 45]. However, unlike MD, individuals with variants in *TONSL* do not have microcephaly and have even lower *Z*-scores for height at older ages as compared to the newborn period suggesting that cell division in chondrocytes in the growth plate may be more severely impacted in this disorder.

In addition to its role in promoting normal replication, it has been shown that TONSL also functions to repair and restart damaged replication forks both through its ability to chaperone histones [46; 47] and to facilitate RAD51 loading [40]. Consequently, transient depletion of TONSL compromises a cell's capacity to replicate through DNA

damage, particularly damage induced by the TOP1 inhibitor, CPT. All three of the subject-derived cell lines exhibited increased levels of spontaneous replication fork stalling and defective formation of CPT-induced RAD51 foci, which could be rescued by the re-expression of wild type *TONSL*. Interestingly, only two out of the three subject-derived cell lines tested exhibited a decreased ability to replicate through CPT-damaged DNA (P6 and P7-1). In contrast, despite exhibiting increased levels of spontaneous replication fork stalling and defective formation of CPT-induced RAD51 foci, the cell line derived from subject 3-1 was able to efficiently replicate in the presence of CPT. Although unexpected, because TONSL has been demonstrated to be required for both processes, it is possible that the variants in P3-1 are 'separation-of-function' variants that disrupt the formation of RAD51 nucleofilaments at one-ended double strand breaks (DSBs) formed upon the CPT-induced collapse of replication forks, while still promoting replication in the presence of CPT via other mechanisms. Indeed, it has been suggested that RAD51, and its associated factors, have both HR-dependent and -independent roles in promoting DNA replication and repair. For example, expression of a dominant negative RAD51 mutant (T131P) does impact the ability of the cells to perform HR, but renders cells unable to efficiently repair DNA inter-strand cross-links[48]. Furthermore, pathogenic variants of the C-terminal RAD51 binding region of BRCA2 specifically compromise its role in protecting replication forks from uncontrolled nucleolytic processing, but still retain its ability to promote efficient HR-mediated repair of DSBs [49]. Therefore, this indicates that an inability of subject-derived cells to form RAD51 foci upon DNA damage is not necessarily indicative of a defect in all RAD51-dependent replication and repair-associated functions,

and that these cellular processes should be tested specifically to ascertain the pathway in which the cellular defect lies.

In addition to its role in dealing with replication-associated DNA damage, TONSL was recently implicated in repairing DNA DSBs [50]. DSBs are predominantly repaired by non-homologous DNA end-joining (NHEJ) in the G1 and G2 phases of the cell cycle but can also be repaired by HR in late S- and G2-phase. Despite being structurally and biochemically distinct, the mechanisms underlying the HR-dependent repair of DSBs and stalled/damaged replication forks share substantial overlap. In a manner similar to replication-associated DNA damage, TONSL-MMS22L has been proposed to be recruited to newly deposited histones at sites of DSB end-resection, where it functions to promote HR by facilitating the loading of RAD51 [50]. Based on this hypothesis, it is tempting to speculate that the more severely affected individuals with *TONSL* variants may have defects in the repair of both replication damage and DNA DSBs, whereas those with a milder clinical phenotype only have deficiencies in one of the TONSL-dependent repair pathways.

It is not currently clear why the *TONSL* variants specifically give rise to skeletal abnormalities. Although skeletal abnormalities, especially short stature or dwarfism, are actually relatively common in human syndromes caused by pathogenic variants in replication fork stability factors or protein involved in responding the replication blocking lesions, the additional skeletal features differ considerably depending on the specific gene that is mutated. For example, a diagnostic clinical feature of Schimke Immunoosseous Dysplasia (SIOD) (MIM: 242900) is spondyloepiphyseal dysplasia. In contrast, Fanconi Anemia (MIM: 227650) is commonly, but not invariably, associated with radial ray

abnormalities and vertebral anomalies. Thus, although normal replication and DNA repair are essential for bone development and growth, a defect in either of these processes does not necessarily give rise to the same specific skeletal abnormalities. Interestingly, however, the skeletal dysplasia phenotype associated with *TONSL* variants, and the variability of the clinical phenotype, seem to share more features in common with SIOD, which is caused by pathogenic variants in the DNA annealing helicase *SMARCAL1* (MIM: 606622), than other replication disorders[43; 51]. Although there have been no reports of SMARCAL1 interacting with or regulating RAD51 directly, it has been shown to promote the reversal of stalled/damaged replication forks, which is a prerequisite for RAD51-dependent fork stabilization. Based on this, it is tempting to speculate that the similarities in skeletal abnormalities exhibited by individuals with *TONSL* and *SMARCAL1* variants are linked to their ability to promote or stabilize reversed replication forks. However, why skeletal development would be particularly affected by loss of this function, which presumably would be essential for many cell types during development, is not known, especially since the expression of *TONSL* appears to be fairly ubiquitous[52]. Only the development of more clinically relevant animal models will be able to answer this question.

Another interesting aspect of the clinical phenotype exhibited by individuals with *TONSL* variants is the immunologic and hematological abnormalities. While hypogammaglobulinemia is often observed in individuals with variants in genes involved in promoting DSB repair such as *NBN* (MIM:602667), *ATM* (MIM:607585), *LIG4* (MIM:601837), *DCLRE1C* (MIM:605988) or *NHEJ1* (MIM:611290), it is not commonly associated with replication deficiency disorders or defects in the HR pathway [53]. This

suggests that perhaps TONSL plays an additional role in facilitating the repair of specialized DSBs, particularly those associated with immune cell maturation and immunoglobulin gene rearrangement. In addition, several subjects exhibited neutropenia. Although this phenotype is relatively rare among both DNA repair and replication disorders, it has been documented in individuals with hypomorphic variants *GINS1* (MIM:610608) and *SMARCAL1*[54]. Currently it is not clear why the neutrophil lineage is specifically sensitive to perturbations in DNA replication. However, the presence of neutropenia in individuals with *TONSL* variants is consistent with its role in repairing damaged replication forks.

Taken together, the findings indicate that the cellular functions of TONSL are essential for cellular viability and that hypomorphic variants in *TONSL* have a deleterious impact at multiple stages of embryonic and postnatal development, particularly during skeletal development. While the underlying reason for the clinical heterogeneity arising from partial loss of TONSL function is unknown, further identification of additional affected individuals will allow us to define the full extent to which variants in this gene affect clinical presentation.

Description of Supplemental Data

The Supplement contains 4 figures and 5 tables.

Consortia

The Undiagnosed Diseases Network co-investigators are David R. Adams, Aaron Aday, Mercedes E. Alejandro, Patrick Allard, Euan A. Ashley, Mahshid S. Azamian, Carlos A.

Bacino, Eva Baker, Ashok Balasubramanyam, Hayk Barseghyan, Gabriel F. Batzli, Alan H. Beggs, Babak Behnam, Hugo J. Bellen, Jonathan A. Bernstein, Gerard T. Berry, Anna Bican, David P. Bick, Camille L. Birch, Devon Bonner, Braden E. Boone, Bret L. Bostwick, Lauren C. Briere, Elly Brokamp, Donna M. Brown, Matthew Brush, Elizabeth A. Burke, Lindsay C. Burrage, Manish J. Butte, Shan Chen, Gary D. Clark, Terra R. Coakley, Joy D. Cogan, Heather A. Colley, Cynthia M. Cooper, Heidi Cope, William J. Craigen, Precilla D'Souza, Mariska Davids, Jean M. Davidson, Jyoti G. Dayal, Esteban C. Dell'Angelica, Shweta U. Dhar, Katrina M. Dipple, Laurel A. Donnell-Fink, Naghmeh Dorrani, Daniel C. Dorset, Emilie D. Douine, David D. Draper, Annika M. Dries, Laura Duncan, David J. Eckstein, Lisa T. Emrick, Christine M. Eng, Gregory M. Enns, Ascia Eskin, Cecilia Esteves, Tyra Estwick, Liliana Fernandez, Carlos Ferreira, Elizabeth L. Fieg, Paul G. Fisher, Brent L. Fogel, Noah D. Friedman, William A. Gahl, Emily Glanton, Rena A. Godfrey, Alica M. Goldman, David B. Goldstein, Sarah E. Gould, Jean-Philippe F. Gourdine, Catherine A. Groden, Andrea L. Gropman, Melissa Haendel, Rizwan Hamid, Neil A. Hanchard, Frances High, Ingrid A. Holm, Jason Hom, Ellen M. Howerton, Yong Huang, Fariha Jamal, Yong-hui Jiang, Jean M. Johnston, Angela L. Jones, Lefkothea Karaviti, David M. Koeller, Isaac S. Kohane, Jennefer N. Kohler, Donna M. Krasnewich, Susan Korrick, Mary Koziura, Joel B. Krier, Jennifer E. Kyle, Seema R. Lalani, C. Christopher Lau, Jozef Lazar, Kimberly LeBlanc, Brendan H. Lee, Hane Lee, Shawn E. Levy, Richard A. Lewis, Sharyn A. Lincoln, Sandra K. Loo, Joseph Loscalzo, Richard L. Maas, Ellen F. Macnamara, Calum A. MacRae, Valerie V. Maduro, Marta M. Majcherska, May Christine V. Malicdan, Laura A. Mamounas, Teri A. Manolio, Thomas C. Markello, Ronit Marom, Martin G. Martin, Julian A. Martínez-Agosto, Shruti Marwaha, Thomas May,

Allyn McConkie-Rosell, Colleen E. McCormack, Alexa T. McCray, Jason D. Merker, Thomas O. Metz, Matthew Might, Paolo M. Moretti, Marie Morimoto, John J. Mulvihill, David R. Murdock, Jennifer L. Murphy, Donna M. Muzny, Michele E. Nehrebecky, Stan F. Nelson, J. Scott Newberry, John H. Newman, Sarah K. Nicholas, Donna Novacic, Jordan S. Orange, James P. Orengo, J. Carl Pallais, Christina GS. Palmer, Jeanette C. Papp, Neil H. Parker, Loren DM. Pena, John A. Phillips III, Jennifer E. Posey, John H. Postlethwait, Lorraine Potocki, Barbara N. Pusey, Genecee Renteria, Chloe M. Reuter, Lynette Rives, Amy K. Robertson, Lance H. Rodan, Jill A. Rosenfeld, Jacinda B. Sampson, Susan L. Samson, Kelly Schoch, Daryl A. Scott, Lisa Shakachite, Prashant Sharma, Vandana Shashi, Rebecca Signer, Edwin K. Silverman, Janet S. Sinsheimer, Kevin S. Smith, Rebecca C. Spillmann, Joan M. Stoler, Nicholas Stong, Jennifer A. Sullivan, David A. Sweetser, Queenie K.-G. Tan, Cynthia J. Tifft, Camilo Toro, Alyssa A. Tran, Tiina K. Urv, Eric Vilain, Tiphanie P. Vogel, Daryl M. Waggott, Colleen E. Wahl, Nicole M. Walley, Chris A. Walsh, Melissa Walker, Jijun Wan, Michael F. Wangler, Patricia A. Ward, Katrina M. Waters, Bobbie-Jo M. Webb-Robertson, Monte Westerfield, Matthew T. Wheeler, Anastasia L. Wise, Lynne A. Wolfe, Elizabeth A. Worthey, Shinya Yamamoto, John Yang, Yaping Yang, Amanda J. Yoon, Guoyun Yu, Diane B. Zastrow, Chunli Zhao, and Allison Zheng.

Acknowledgements

We sincerely thank the subjects and their families for participation. We thank Dr. Xiangli Yang, Alyssa Tran, Mercedes Alejandro, Brian Dawson, Dr. David Murdock, and Dr. Huan-Chang Zeng for their technical assistance. We would also like to thank Professors

Daniel Durocher, Peter Cejka and John Rouse for kindly gifting their anti-TONSL and anti-MMS22L antibodies and expression plasmids, and Dr. Yonghwan Kim for the lentiviral construct expressing Flag-*TONSL*. This work was supported by NIH U01HG007709 (BL), NIH UM1HG006348 (AB, MD, JDH), NIH U54NS093793 (JP, JW, MW), NIH U54HG006493 (MB), NIH R01AI120989 (JSO), University of Utah Pathology Departmental Funds (CC), ARUP Laboratories Roberts Memorial Fund Research Award (CC), NIH K08DK106453 (LCB), and a Career Award for Medical Scientists from the Burroughs Wellcome Fund (LCB). In addition, funding was received by NIH/NIGMS T32GM007526 to BL, NIH/NICHD U54HD083092 for the Baylor College of Medicine Intellectual and Developmental Disabilities Research Center (IDDRC), and from the Canadian Institutes of Health Research (CIHR), the Fonds de recherche du Québec – Santé (FRQS) and the Quebec Network for Oral and Bone Health Research (RSBO) to PMC to study rare skeletal dysplasias. JJR and GSS are funded by a CR-UK Programme Grant (C17183/A23303) and the University of Birmingham. MRH is funded by an MRC Career Development Fellowship (MR/P009085/1) and the University of Birmingham. . APJ is supported by the Medical Research Council UK (MRC, U127580972) and the European Research Council (ERC); and the European Union's Horizon 2020 research and innovation programme ERC Advanced Grant (grant agreement No: 788093). Support for DHC and DK was provided in part by NIH Awards RO1AR062651 and R01AR066124. The "Cell Line and DNA Biobank from Patients Affected by Genetic Diseases", member of the Telethon Network of Genetic Biobanks (project no. GTB18001), funded by Telethon Italy, provided us with specimens for subject 11. Support for DRB was provided by

FAPESP 2015/21783-9/CEPID 2013/08028-1; CNPq 304130/2016-8. See Supplemental Acknowledgments for consortium details.

Web Resources

1000 Genomes, http://browser.1000genomes.org

Clinvar, https://www.ncbi.nlm.nih.gov/clinvar/

CADD, http://cadd.gs.washington.edu/

Codified Genomics, http://codifiedgenomics.com/

dbSNP, https://www.ncbi.nlm.nih.gov/projects/SNP/

ExAC, http://exac.broadinstitute.org/

gnomAD, http://gnomad.broadinstitute.org/

GTEX Portal, https://gtexportal.org/home/

HGSC Mercury Analysis Pipeline, https://www.hgsc.bcm.edu/software/mercury

Human Splice Finder 3.1, http://www.umd.be/HSF3/

HGMD, http://www.hgmd.cf.ac.uk/ac/index.php

KOMP2, http://www.mousephenotype.org/data/genes

Mercury pipeline, https://www.hgsc.bcm.edu/software/mercury

Mutation Taster, http://www.mutationtaster.org/

OMIM, http://www.omim.org/

Polyphen-2, http://genetics.bwh.harvard.edu/pph2/

Sift, http://sift.jcvi.org

ZiFiT Targeter software, http://zifit.partners.org/ZiFiT/

Declaration of Interests

The Department of Molecular and Human Genetics at Baylor College of Medicine derives revenue from clinical laboratory testing conducted at Baylor Genetics. Dr. Brendan Lee serves on the Board of Directors of Baylor Genetics and chairs it Scientific Advisory Board but receives no personal income from these positions.

References

1. Fanconi, S., Issler, C., Giedion, A., and Prader, A. (1983). The SPONASTRIME dysplasia: familial short-limb dwarfism with saddle nose, spinal alterations and metaphyseal striation. Report of 4 siblings. Helvetica paediatrica acta 38, 267-280.
2. Langer, L.O., Jr., Beals, R.K., LaFranchi, S., Scott, C.I., Jr., and Sockalosky, J.J. (1996). Sponastrime dysplasia: five new cases and review of nine previously published cases. American journal of medical genetics 63, 20-27.
3. Masuno, M., Nishimura, G., Adachi, M., Hotsubo, T., Tachibana, K., Makita, Y., Imaizumi, K., and Kuroki, Y. (1996). SPONASTRIME dysplasia: report on a female patient with severe skeletal changes. American journal of medical genetics 66, 429-432.
4. Cooper, H.A., Crowe, J., and Butler, M.G. (2000). SPONASTRIME dysplasia: report of an 11-year-old boy and review of the literature. American journal of medical genetics 92, 33-39.
5. Umpaichitra, V., Wallerstein, R., and Castells, S. (2002). Sponastrime dysplasia with abnormal urinary glycosaminoglycans and growth hormone unresponsiveness. Clinical dysmorphology 11, 53-56.
6. Lachman, R.S., Stoss, H., and Spranger, J. (1989). Sponastrime dysplasia. A radiologic-pathologic correlation. Pediatric radiology 19, 417-424.
7. Gripp, K.W., Johnson, C., Scott, C.I., Jr., Nicholson, L., Bober, M., Butler, M.G., Shaw, L., and Gorlin, R.J. (2008). Expanding the phenotype of SPONASTRIME dysplasia to include short dental roots, hypogammaglobulinemia, and cataracts. American journal of medical genetics Part A 146A, 468-473.
8. Offiah, A.C., Lees, M., Winter, R.M., and Hall, C.M. (2001). Sponastrime dysplasia: presentation in infancy. Journal of medical genetics 38, 889-893.
9. Nishimura, G., Mikawa, M., and Fukushima, Y. (1998). Another observation of Langer-type sponastrime dysplasia variant. American journal of medical genetics 80, 288-290.
10. Langer, L.O., Jr., Beals, R.K., and Scott, C.I., Jr. (1997). Sponastrime dysplasia: diagnostic criteria based on five new and six previously published cases. Pediatric radiology 27, 409-414.
11. Filocamo, M.e.a. (2014). Cell line and DNA biobank from patients affected by genetic diseases. Open Journal of Bioresources.
12. Bainbridge, M.N., Wang, M., Wu, Y., Newsham, I., Muzny, D.M., Jefferies, J.L., Albert, T.J., Burgess, D.L., and Gibbs, R.A. (2011). Targeted enrichment beyond the consensus coding DNA sequence exome reveals exons with higher variant densities. Genome biology 12, R68.

13. Challis, D., Yu, J., Evani, U.S., Jackson, A.R., Paithankar, S., Coarfa, C., Milosavljevic, A., Gibbs, R.A., and Yu, F. (2012). An integrative variant analysis suite for whole exome next-generation sequencing data. BMC bioinformatics 13, 8.
14. Reid, J.G., Carroll, A., Veeraraghavan, N., Dahdouli, M., Sundquist, A., English, A., Bainbridge, M., White, S., Salerno, W., Buhay, C., et al. (2014). Launching genomics into the cloud: deployment of Mercury, a next generation sequence analysis pipeline. BMC bioinformatics 15, 30.
15. Li, H., and Durbin, R. (2010). Fast and accurate long-read alignment with Burrows-Wheeler transform. Bioinformatics 26, 589-595.
16. McKenna, A., Hanna, M., Banks, E., Sivachenko, A., Cibulskis, K., Kernytsky, A., Garimella, K., Altshuler, D., Gabriel, S., Daly, M., et al. (2010). The Genome Analysis Toolkit: a MapReduce framework for analyzing next-generation DNA sequencing data. Genome research 20, 1297-1303.
17. Li, H., Handsaker, B., Wysoker, A., Fennell, T., Ruan, J., Homer, N., Marth, G., Abecasis, G., Durbin, R., and Genome Project Data Processing, S. (2009). The Sequence Alignment/Map format and SAMtools. Bioinformatics 25, 2078-2079.
18. Kumar, P., Henikoff, S., and Ng, P.C. (2009). Predicting the effects of coding non-synonymous variants on protein function using the SIFT algorithm. Nature protocols 4, 1073-1081.
19. Adzhubei, I.A., Schmidt, S., Peshkin, L., Ramensky, V.E., Gerasimova, A., Bork, P., Kondrashov, A.S., and Sunyaev, S.R. (2010). A method and server for predicting damaging missense mutations. Nature methods 7, 248-249.
20. Schwarz, J.M., Cooper, D.N., Schuelke, M., and Seelow, D. (2014). MutationTaster2: mutation prediction for the deep-sequencing age. Nature methods 11, 361-362.
21. Reynolds, J.J., Bicknell, L.S., Carroll, P., Higgs, M.R., Shaheen, R., Murray, J.E., Papadopoulos, D.K., Leitch, A., Murina, O., Tarnauskaite, Z., et al. (2017). Mutations in DONSON disrupt replication fork stability and cause microcephalic dwarfism. Nature genetics 49, 537-549.
22. Yang, Y., Muzny, D.M., Xia, F., Niu, Z., Person, R., Ding, Y., Ward, P., Braxton, A., Wang, M., Buhay, C., et al. (2014). Molecular findings among patients referred for clinical whole-exome sequencing. Jama 312, 1870-1879.
23. Sukenik Halevy, R., Chien, H.C., Heinz, B., Bamshad, M.J., Nickerson, D.A., University of Washington Center for Mendelian, G., Kircher, M., and Ahituv, N. (2018). Mutations in the fourth beta-propeller domain of LRP4 are associated with isolated syndactyly with fusion of the third and fourth fingers. Hum Mutat 39, 811-815.
24. Lopes, F., Miguet, M., Mucha, B.E., Gauthier, J., Saillour, V., Nguyen, C.E., Vanasse, M., Ellezam, B., Michaud, J.L., Soucy, J.F., et al. (2018). MYOD1 involvement in myopathy. European journal of neurology 25, e123-e124.
25. Hodgkins, A., Farne, A., Perera, S., Grego, T., Parry-Smith, D.J., Skarnes, W.C., and Iyer, V. (2015). WGE: a CRISPR database for genome engineering. Bioinformatics 31, 3078-3080.
26. Bassett, A.R., Tibbit, C., Ponting, C.P., and Liu, J.L. (2013). Highly efficient targeted mutagenesis of Drosophila with the CRISPR/Cas9 system. Cell reports 4, 220-228.
27. Westerfield, M. (2007). The zebrafish book : a guide for the laboratory use of zebrafish (Danio rerio).(Eugene, OR: The University of Oregon Press).
28. Renshaw, S.A., Loynes, C.A., Trushell, D.M., Elworthy, S., Ingham, P.W., and Whyte, M.K. (2006). A transgenic zebrafish model of neutrophilic inflammation. Blood 108, 3976-3978.
29. Liu, D., Wang, Z., Xiao, A., Zhang, Y., Li, W., Zu, Y., Yao, S., Lin, S., and Zhang, B. (2014). Efficient gene targeting in zebrafish mediated by a zebrafish-codon-optimized cas9 and

evaluation of off-targeting effect. Journal of genetics and genomics = Yi chuan xue bao 41, 43-46.
30. Walker, M.B., and Kimmel, C.B. (2007). A two-color acid-free cartilage and bone stain for zebrafish larvae. Biotechnic & histochemistry : official publication of the Biological Stain Commission 82, 23-28.
31. Stewart, G.S., Maser, R.S., Stankovic, T., Bressan, D.A., Kaplan, M.I., Jaspers, N.G., Raams, A., Byrd, P.J., Petrini, J.H., and Taylor, A.M. (1999). The DNA double-strand break repair gene hMRE11 is mutated in individuals with an ataxia-telangiectasia-like disorder. Cell 99, 577-587.
32. O'Donnell, L., Panier, S., Wildenhain, J., Tkach, J.M., Al-Hakim, A., Landry, M.C., Escribano-Diaz, C., Szilard, R.K., Young, J.T., Munro, M., et al. (2010). The MMS22L-TONSL complex mediates recovery from replication stress and homologous recombination. Molecular cell 40, 619-631.
33. Sobreira, N., Schiettecatte, F., Valle, D., and Hamosh, A. (2015). GeneMatcher: a matching tool for connecting investigators with an interest in the same gene. Hum Mutat 36, 928-930.
34. Kircher, M., Witten, D.M., Jain, P., O'Roak, B.J., Cooper, G.M., and Shendure, J. (2014). A general framework for estimating the relative pathogenicity of human genetic variants. Nature genetics 46, 310-315.
35. Szafranski, P., Karolak, J.A., Lanza, D., Gajecka, M., Heaney, J., and Stankiewicz, P. (2017). CRISPR/Cas9-mediated deletion of lncRNA Gm26878 in the distant Foxf1 enhancer region. Mammalian genome : official journal of the International Mammalian Genome Society 28, 275-282.
36. Lanza, D.G., Gaspero, A., Lorenzo, I., Liao, L., Zheng, P., Wang, Y., Deng, Y., Cheng, C., Zhang, C., Seavitt, J.R., et al. (2018). Comparative analysis of single-stranded DNA donors to generate conditional null mouse alleles. BMC biology 16, 69.
37. O'Connell, B.C., Adamson, B., Lydeard, J.R., Sowa, M.E., Ciccia, A., Bredemeyer, A.L., Schlabach, M., Gygi, S.P., Elledge, S.J., and Harper, J.W. (2010). A genome-wide camptothecin sensitivity screen identifies a mammalian MMS22L-NFKBIL2 complex required for genomic stability. Molecular cell 40, 645-657.
38. Duro, E., Lundin, C., Ask, K., Sanchez-Pulido, L., MacArtney, T.J., Toth, R., Ponting, C.P., Groth, A., Helleday, T., and Rouse, J. (2010). Identification of the MMS22L-TONSL complex that promotes homologous recombination. Molecular cell 40, 632-644.
39. Piwko, W., Olma, M.H., Held, M., Bianco, J.N., Pedrioli, P.G., Hofmann, K., Pasero, P., Gerlich, D.W., and Peter, M. (2010). RNAi-based screening identifies the Mms22L-Nfkbil2 complex as a novel regulator of DNA replication in human cells. The EMBO journal 29, 4210-4222.
40. Piwko, W., Mlejnkova, L.J., Mutreja, K., Ranjha, L., Stafa, D., Smirnov, A., Brodersen, M.M., Zellweger, R., Sturzenegger, A., Janscak, P., et al. (2016). The MMS22L-TONSL heterodimer directly promotes RAD51-dependent recombination upon replication stress. The EMBO journal 35, 2584-2601.
41. Techer, H., Koundrioukoff, S., Azar, D., Wilhelm, T., Carignon, S., Brison, O., Debatisse, M., and Le Tallec, B. (2013). Replication dynamics: biases and robustness of DNA fiber analysis. Journal of molecular biology 425, 4845-4855.
42. Nieminuszczy, J., Schwab, R.A., and Niedzwiedz, W. (2016). The DNA fibre technique - tracking helicases at work. Methods 108, 92-98.
43. Boerkoel, C.F., Takashima, H., John, J., Yan, J., Stankiewicz, P., Rosenbarker, L., Andre, J.L., Bogdanovic, R., Burguet, A., Cockfield, S., et al. (2002). Mutant chromatin remodeling protein SMARCAL1 causes Schimke immuno-osseous dysplasia. Nature genetics 30, 215-220.

44. Mo, D., Zhao, Y., and Balajee, A.S. (2018). Human RecQL4 helicase plays multifaceted roles in the genomic stability of normal and cancer cells. Cancer letters 413, 1-10.
45. Harley, M.E., Murina, O., Leitch, A., Higgs, M.R., Bicknell, L.S., Yigit, G., Blackford, A.N., Zlatanou, A., Mackenzie, K.J., Reddy, K., et al. (2016). TRAIP promotes DNA damage response during genome replication and is mutated in primordial dwarfism. Nature genetics 48, 36-43.
46. Saredi, G., Huang, H., Hammond, C.M., Alabert, C., Bekker-Jensen, S., Forne, I., Reveron-Gomez, N., Foster, B.M., Mlejnkova, L., Bartke, T., et al. (2016). H4K20me0 marks post-replicative chromatin and recruits the TONSL-MMS22L DNA repair complex. Nature 534, 714-718.
47. Campos, E.I., Smits, A.H., Kang, Y.H., Landry, S., Escobar, T.M., Nayak, S., Ueberheide, B.M., Durocher, D., Vermeulen, M., Hurwitz, J., et al. (2015). Analysis of the Histone H3.1 Interactome: A Suitable Chaperone for the Right Event. Molecular cell 60, 697-709.
48. Wang, A.T., Kim, T., Wagner, J.E., Conti, B.A., Lach, F.P., Huang, A.L., Molina, H., Sanborn, E.M., Zierhut, H., Cornes, B.K., et al. (2015). A Dominant Mutation in Human RAD51 Reveals Its Function in DNA Interstrand Crosslink Repair Independent of Homologous Recombination. Molecular cell 59, 478-490.
49. Schlacher, K., Christ, N., Siaud, N., Egashira, A., Wu, H., and Jasin, M. (2011). Double-strand break repair-independent role for BRCA2 in blocking stalled replication fork degradation by MRE11. Cell 145, 529-542.
50. Huang, T.H., Fowler, F., Chen, C.C., Shen, Z.J., Sleckman, B., and Tyler, J.K. (2018). The Histone Chaperones ASF1 and CAF-1 Promote MMS22L-TONSL-Mediated Rad51 Loading onto ssDNA during Homologous Recombination in Human Cells. Molecular cell 69, 879-892 e875.
51. Hunter, K.B., Lucke, T., Spranger, J., Smithson, S.F., Alpay, H., Andre, J.L., Asakura, Y., Bogdanovic, R., Bonneau, D., Cairns, R., et al. (2010). Schimke immunoosseous dysplasia: defining skeletal features. European journal of pediatrics 169, 801-811.
52. Consortium, G.T. (2013). The Genotype-Tissue Expression (GTEx) project. Nature genetics 45, 580-585.
53. Morio, T. (2017). Recent advances in the study of immunodeficiency and DNA damage response. International journal of hematology 106, 357-365.
54. Cottineau, J., Kottemann, M.C., Lach, F.P., Kang, Y.H., Vely, F., Deenick, E.K., Lazarov, T., Gineau, L., Wang, Y., Farina, A., et al. (2017). Inherited GINS1 deficiency underlies growth retardation along with neutropenia and NK cell deficiency. The Journal of clinical investigation 127, 1991-2006.
55. Jian, X., Boerwinkle, E., and Liu, X. (2014). In silico prediction of splice-altering single nucleotide variants in the human genome. Nucleic acids research 42, 13534-13544.
56. Desmet, F.O., Hamroun, D., Lalande, M., Collod-Beroud, G., Claustres, M., and Beroud, C. (2009). Human Splicing Finder: an online bioinformatics tool to predict splicing signals. Nucleic acids research 37, e67.

Figures

Figure 1. *TONSL* variants in subjects with skeletal dysplasias**.** (A) Subject photographs and radiographs. The characteristic facial features of SPONASTRIME dysplasia (midface hypoplasia and depressed nasal root) are more evident in subjects 2, 3-1, and 4. Characteristic features of the spine are demonstrated with biconcave vertebrae in subject 4, 7-1, and 7-2 and platyspondyly

in subjects 2, 3-1 and 4. Metaphyseal striations are most evident in subjects 3-1 and 4. (B) Pathogenic variants identified in subjects with various skeletal dysplasias. (C) Immunoblot demonstrating reduced protein in subject 6 (P6) with apparently normal protein levels in subjects 7-1 (P7-1) and 3-1 (P3-1). DNA-PKcs was used as a loading control. The x-ray showing the metaphyseal striations in subject 4 is reproduced from [Sponastrime dysplasia: presentation in infancy, *Journal of Medical Genetics*, Offiah AC, Lees M, Winter RM, and Hall CM, 38, 889-93, 2001] with permission from BMJ Publishing Group Ltd.

Figure 2. (A) *tonsl*$^{-/-}$ zebrafish are larval lethal and show progressively diminished size compared to wild-type siblings. Food intake is variable in mutants and correlated with reduced fitness and mortality (gut contents indicated with white arrows). (B) *tonsl*$^{-/-}$ fish (red) are not significantly smaller than wild-type siblings (blue) at 6 dpf (days post fertilization) or 8 dpf, but are on average smaller at later timepoints through 13 dpf ($N \geq 10$ larvae for each timepoint; $p = 0.045$ at 10 dpf; $p < .0001$ at 13 dpf). Normal zebrafish growth during this stage varies widely, and survivor bias is a factor in these data as *tonsl*$^{-/-}$ mutants begin to die at 8 dpf. (C) *tonsl* mutants exhibit precocious ossification of the axial skeleton. Bone formation is visualized by staining with Alizarin red, and cartilage is stained with Alcian blue. At 7 dfp, vertebral development is marked by bony centra forming around the notochord (asterisks). Significantly more centra have formed by this stage in homozygous *tonsl* mutants compared to wild type siblings. WT: 4.100 ± 0.5667, n=10; *tonsl*$^{-/-}$: 8.867 ± 0.4350, n=15 larvae. (D) Wild type larvae have a high concentration of neutrophils in the gut (dashed outline) and neutrophils are dispersed throughout the circulatory system (D^{o}). *mpo:gfp*;*tonsl*$^{-/-}$ mutants have variable neutrophil distribution correlated with their decline in health, ranging from normal (D') to reduced neutrophil fluorescence in the

gut (D'', D'''), to diminished numbers of circulating neutrophils observable in blood vessels of the head and trunk (D'''). (E) The number of circulating neutrophils in *mpo:gfp*;*tonsl*$^{-/-}$ is reduced in mutants showing signs of decline (D''', red) compared to stage-matched wild type (blue). Gut neutrophils were excluded from this count (N = 10; $p < .0001$). Scale bars in A, D: 1mm; in C: 500nm. Student's t-tests with Welch's Correlation were performed for each data set. Data in (B) is mean +/- SD.

Figure 3. Impact of *TONSL* variants on CPT-induced RAD51 foci formation. (A) Cell lines derived from individuals with biallelic *TONSL* variants exhibit defective recruitment of RAD51 foci to CPT induced DNA damage. RAD51 foci formation was analyzed by immunofluorescence in subject-derived fibroblasts exposed to 1 μM CPT, and the percentage of cells with pan-nuclear γH2AX staining with 'strong' RAD51 foci was quantified. ATLD2 is a fibroblast cell line derived from an individual with a confirmed genetic diagnosis of ataxia telangiectasia-like disorder (pathogenic variants in *MRE11*) and was used as a control. N = 3 independent experiments. A minimum of 400 cells were counted per experiment. For statistical analysis, Student's T-Test was performed (** = $p < 0.01$, *** = $p < 0.001$). Data in (A) show mean values and error bars denote SEM, and representative images are shown in (B).

Figure 4. Cell lines from individuals with biallelic *TONSL* variants exhibit increased levels of spontaneous replication fork stalling, and defective replication fork progression in the presence of CPT. (A) Schematic for DNA fiber analysis in the absence or presence of exogenous replication stress. Subject-derived cell lines were pulsed with CldU for 30

minutes, and then pulsed with IdU, or IdU with 50 nM CPT, for 30 minutes. (B) DNA fiber analysis on subject-derived fibroblast cell lines. The percentage of ongoing forks (left) or stalled forks (right) in the absence of exogenous DNA damage were quantified. Representative images of ongoing forks and stalled forks are included below. A minimum of 850 fork structures in total were counted over 3 independent experiments. For statistical analysis, Student's T-Test was performed. Error bars denote SEM. (C) Dot density graph representation of the ratio of IdU tract length / CldU tract length in untreated and CPT treated patient-derived fibroblasts. N = 3 independent experiments. A minimum of 100 ongoing fork structures were counted per experiment. Red lines denote mean values. For statistical analysis, Mann-Whitney rank sum test was performed. In all cases * = $p < 0.01$, ** = $p < 0.01$ and *** = $p < 0.001$.

Figure 5. Wild Type TONSL rescues CPT-induced RAD51 foci formation and corrects the replication abnormalities observed in subject-derived fibroblasts. (A) Representative immunoblot analysis of TONSL in fibroblasts derived from subjects P3-1 and P6 infected with lentiviruses encoding wild type Flag-tagged TONSL or an empty vector. DNA-PKcs was used as a loading control. (B and C) Fibroblasts cell lines from (A) were exposed to 1μM CPT, and the percentage of cells with RAD51 foci formation was quantified as in Figure 3A. A minimum of 1000 cells in total were counted over 3 independent experiments. For statistical analysis, Student's T-Test was performed. Error bars denote SEM. Representative images are shown in (B). (D) DNA fiber analysis was performed on subject-derived fibroblasts cell lines expressing either Flag-tagged wild type TONSL or an empty lentiviral vector. The percentage of stalled forks in untreated cells was

quantified. A minimum of 350 fork structures in total were counted over 3 independent experiments. For statistical analysis, Student's T-Test was performed. Error bars denote SEM. (E) Dot density graph representation of the ratio of IdU tract length / CldU tract length in CPT treated fibroblasts. A minimum of 200 fork structures in total were counted over 3 independent experiments. For statistical analysis, Mann-Whitney rank sum test was performed. Red lines denote mean values. In all cases: *** = $p < 0.001$; ** = $p < 0.01$.

Figure 6. Subject-derived fibroblasts exhibit increased levels of spontaneous chromosomal aberrations. (A) Metaphase spreads were prepared from subject-derived fibroblast cell lines expressing either Flag-tagged wild type TONSL or an empty lentiviral vector. The average number of spontaneous chromosomal aberrations per metaphase was quantified. N = 3 independent experiments. A minimum of 32 metaphases were counted for each experiment. For statistical analysis, Student's T-Test was performed (*** = $p < 0.001$). Error bars denote SEM. Representative images of metaphase spreads are shown in (B).

Table 1. Skeletal Features of Subjects Diagnosed with SPONASTRIME Dysplasia

Subject ID	1	2	3-1	3-2	4	5	13	14	15
Sex	F	F	M	M	F	F	M	F	M
Age at last follow-up	7 y 9 m	7 y 11 m	4 y 9 m	9 m	22 y	23 y	17 y 10 m	4 y	11 y
Height (Z-score)	-3.3	-4.2	-5.0	-9.0	-10.8	-8.8	-5.1	-6.7	-6.0
Weight (Z-score)	-0.1	-1.2	-2.1	-5.1	-4.2	-3.0	-2.4	-2.2	-4.0
FOC (Z-score)	Not available	Not available	-0.6	Not available	-3.4	-2.1	0.6	-1.0	-3.0
Disproportionate Short Stature	Yes	Yes	Yes	Yes	Yes	Yes	No	Yes	Yes
Orthopedic Abnormalities	None	Genu valgum; Leg length discrepancy; Perthes vs. avascular necrosis[a]	Rhizomelia; Brachydactyly	Rhizomelia; Brachydactyly	Rhizomelia and mesomelia; Short, broad hands and feet	Mildly short hands and feet	Knee pain but no surgeries or joint dislocations	Kyphoscoliosis; Hyperlordosis; Joint laxity; Genu valgus	Genu valgum (s/p surgery); Leg length discrepancy, Brachydactyly
Radiographic Features									
Metaphyses	Widened metaphyses with striations and irregularities	Metaphyseal irregularities	Broad, flared with striations and irregularities	Broad and flared	Metaphyseal striations with irregularities	Widened metaphyses with striations and irregularities	Irregular, with striations	Metaphyseal striations with irregularities	Striations and irregularities, most notably in distal femurs and proximal tibias
Epiphyses	Normal	Unknown	Small epiphyses which progressed to flattened epiphyses	Normal	Unknown	Normal	Normal	Normal	Small, delayed ossification
Spine	Platyspondyly	Platyspondyly	Platyspondyly	Platyspondyly	Platyspondyly with biconcave vertebrae; Progressive severe double curve scoliosis	Platyspondyly; Biconcave vertebrae	Biconcave vertebrae with mild platyspondyly	Mild platyspondyly; Some vertebral bodies with biconcave endplates	Biconcave deformities; Pear-shaped vertebral bodies; Progressive decrease in interpedicular distances
Other Skeletal Findings	Short, wide femoral necks	Unknown	Shallow acetabula with prominent ischial component; Genu valgum	Squaring of iliac wings	Very short, irregular femoral necks; Coxa vara; Ivory epiphyses (hand); Dislocated left hip with pseudoacetabulum	Short femoral neck; Coxa vara	Exaggerated lumbar lordosis	None	Slightly short and wide femoral necks

[a]Reported by parents after evaluation.

Table 2. Variants in *TONSL* in Subjects with Clinical Diagnosis of SPONASTRIME Dysplasia

Family ID	1	2	3	4	5	13	14	15
Variant 1	c.2800C>T, p.(Arg934Trp)	c.1459G>A, p.(Glu487Lys)	c.2800C>T, p.(Arg934Trp)	c.1480G>A, p.(Glu494Lys)	c.1459G>A p.Glu487Lys	c.3096dupA, p.(Gln1033Thrfs*57)	c.2800C>T p.(Arg934Trp)	c.2800C>T, p.(Arg934Trp)
rsID	rs755575416	rs563710728	rs755575416	rs775551492	rs563710728	N/A	rs7555754	rs755575416
Frequency (gnomAD)	1 / 150710	21 / 239692	1 / 150710	1 / 30966	21 / 239692	Not present	1 / 150710	1 / 150710
Polyphen	Probably damaging	Probably damaging	Probably damaging	Benign	Probably damaging	N/A	Probably damaging	Probably damaging
Sift	Damaging	Damaging	Damaging	Tolerated	Damaging	N/A	Damaging	Damaging
CADD	16.77	21.3	16.77	16.12	21.3	N/A	16.77	16.77
Variant2	c.460C>T, p.(Gln154*)	c.1602_1612del, p.(Ala536Glyfs*17)	c.3589T>C, p.(Ser1197Pro)	c.2638_2647delinsGG, p.(Arg880Glyfs*10)	c.1864dup p.Ala622Glyfs*67	c.122-5C>G	c.3796dupA, p.(Arg1266Lysfs*23)	c.2407C>T (p.Gln803*)
rsID	rs1026265047	N/A	N/A	N/A	rs762903420	N/A	rs782733226	rs769100855
Frequency (gnomAD)	2 / 243938	Not present	Not present	Not present	Not present	Not present	2 / 251402	2 / 219724
Polyphen	N/A	N/A	Probably damaging	N/A	N/A	N/A	N/A	N/A
Sift	N/A	N/A	Damaging	N/A	N/A	N/A	N/A	N/A
CADD	N/A	N/A	15.56	N/A	N/A	N/A	N/A	N/A

All coordinates utilize hg19, NM_013432.4. Parental DNA for subjects 13 and 15 were not available to ascertain segregation. Variant c.122-5C>G was assessed using dbscSNV [55] and Human Splicing Finder 3.1 [56] but the effects did not reach statistical significance.

Table 3. Skeletal Features for Subjects Without a Clinical Diagnosis of SPONASTRIME Dysplasia

Subject ID	6	7-1	7-2	8
Diagnosis	Spondylometaphyseal Dysplasia	Spondylometaphyseal Dysplasia	Spondylometaphyseal Dysplasia	Spondylometaphyseal Dysplasia
Sex	F	F	M	F
Age at last follow-up	12 y	10 y 9 m	9 y 9 m	5 y 11 m
Height (Z-score)	-10.6	-1.5	-1.6	-6.5
Weight (Z-score)	-5.1	-0.2	0.8	-5.3
FOC (Z-score)	-8.0	0.1	-1.0	-4.3
Disproportionate short stature	No	No	No	Yes
Orthopedic Abnormalities	Long tapering fingers and proximally inserted thumbs; Long and overlapping toes	Pes planus	None	Rhizomelia and mesomelia; 5^{th} finger clinodactyly
Radiographic Features				
Metaphyses	Irregular	Mild metaphyseal irregularities with mild striations	Mild widening and irregularities with mild striations	Broad, flared, and irregular metaphyses with mild striations
Epiphyses	Normal	Normal	Normal	Normal
Spine	Platyspondyly	Biconcave vertebrae	Biconcave vertebrae	Platyspondyly
Other Skeletal Findings	None	Short, wide, femoral necks	Short, wide, femoral necks	Squaring of iliac wings; Coxa valga

Table 4. Variants in *TONSL* in Subjects without a Clinical Diagnosis of SPONASTRIME Dysplasia

Family ID	6	7	8
Variant 1	c.2137C>T, p.(Gln713*)	c.866-1G>C	c.329G>A, p.(Trp110*)
rsID	N/A	N/A	N/A
Frequency (gnomAD)	Not present	Not present	Not present
Polyphen	N/A	N/A	N/A
Sift	N/A	N/A	N/A
CADD	N/A	11.62	N/A
Variant2	c.1958C>T, p.(Thr653Met)	c.595G>A, p.(Glu199Lys)	c.1837G>T, p.(Val613Leu)
rsID	rs755055463	N/A	N/A
Frequency (gnomAD)	4 / 244636	Not present	Not present
Polyphen	Probably damaging	Probably damaging	Probably damaging
Sift	Damaging	Damaging	Damaging
CADD	20.8	36	21.5

All coordinates utilize hg19, NM_013432.4. Variant c.866-1G>C is predicted to affect splicing by dbscSNV [55] and Human Splicing Finder 3.1. [56]

Table 5. Early embryonic lethality in *Tonsl*$^{-/-}$ mouse

	Postnatal Day 14	Embryonic Day 9.5
***Tonsl*$^{+/+}$**	59	7
***Tonsl*$^{+/-}$**	125	26
***Tonsl*$^{-/-}$**	0	0
Chi square, df	52.63, 2	10.43, 2
p value	<0.0001	0.0054

Table S1. Primers used for Sanger sequencing of human *TONSL*

Exons	5' primer	3' primer	Amplicon size (nt)
hTONSLex1-2	GGCCGACCGTACTTCCC	CTCCTGCCAGTGCTGCTC	636
hTONSLex3	CAAGGCGAAAGCCAAGG	AACCTACTCCTGCCCCAGTC	586
hTONSLex4	AGCAAGAACAGGGTCTCTGG	GCTCCAGAAGACGGGATTG	373
hTONSLex5	GGCCCAAAGCTGGAAAC	ACTTCCTCCAGGAACAAGGG	249
hTONSLex6-7	CCGTGTGGCATCAGCAG	GGCTCACCCCTGCACAC	492
hTONSLex8-9	TCACAGCTTGCAGGTGGTAG	GTCCTGAGGCAGAGACATGG	524
hTONSLex10-11	CCGTTGGACGCAGACAG	CACAGCACACCCCTCTCC	578
hTONSLex12-13	CTGCTAACCTTCACCTCCC	CACAAACGCACAGCTCCTC	380
hTONSLex14-15	TAGGCTGCAGAGCTCACG	AGTTGAGCAGGGGCACAG	483
hTONSLex16	ACTCGAAAGGTGAGCCTGG	CGGGGACTCTCAGCGTAG	263
hTONSLex17_1	GATGCTCCATCACAGGTGG	AAGGGCTTTGCTGTGGC	508
hTONSLex17_2	ACAGGGAAGCAGCCACAG	AGTGGGCTCCACCCTACAC	509
hTONSLex18	AGGCAGGTGTAGGGTGGAG	ACCCTGACATGCAAACACG	217
hTONSLex19-20	GCATTACCCCGGCTGTG	TGGTGGAGCCTGTGTGC	481
hTONSLex21	GATTCAGAGGGCAGAAAGGG	GGACCTGCAGAATGGGAAC	423
hTONSLex22	GACTGCCAAGCCAAGCC	GTCCTGGAAACCCTCAATGC	312
hTONSLex23	AGAACTTGGGGTGGGTACAG	GAGCTCCTCCCAGCAACC	313
hTONSLex24	TGCTGGGAAGCAGGCAG	CCTTCTCCCATAGGGTCCAG	212
hTONSLex25	GCAGCTTTCCTAGTGTTGGG	CACCTGGGTCTCAGGCAG	274
hTONSLex26	TCCTGGCATCTGTACCTTCC	AAGCCCGGTCTTACCCC	1008

Table S2. Additional Subject Characteristics for Subjects with Clinical Diagnosis of SPONASTRIME Dysplasia

Subject ID	1	2	3-1	3-2	4	5	13	14	15
Sex	F	F	M	M	F	F	M	F	M
Age at last follow-up	7 y 9 m	7 y 11 m	4 y 9 m	9 m	22 y	23 y	17 y 10 m	4 y	11 y
Birth Parameters									
Gestational Age	Not available	Full term	40 weeks	40 weeks	40 weeks	38 weeks	Full term	39 weeks	39 weeks
Length	Not available	-3.71	-1.16	-3.41	-2.83	-1.89	Not available	-0.23	-2.94
Weight	Not available	-2.70	-4.71	-1.78	-2.18	-1.01	Not available	-2.03	-2.11
FOC	Not available	Not available	Not available	-0.38	-2.32	-0.41	Not available	-2.26	Not available
Extra-Skeletal Features									
Dental	Unknown	Short dental roots; Malocclusion with early loss of teeth[a]	Normal	None	Shallow dental roots	Malocclusion ; Early loss of teeth; Gingival recession	Normal examination	Short dental roots	Short dental roots; Dental crowding
Facial Features	Midface hypoplasia	Midface hypoplasia; Prominent forehead	Midface hypoplasia; Frontal bossing	Midface hypoplasia; Prominent forehead	Midface hypoplasia; Frontal bossing; Short philtrum	Midface hypoplasia; Prominent forehead	Midface hypoplasia	Frontal bossing; Midface hypoplasia	Coarse, mid face hypoplasia; Flat, depressed nasal bridge; Short upturned nose and thick full lips; Frontal bossing; Mild dolichocephaly with maxillary hypoplasia
Eye	Unknown	Bilateral cataracts (age ~10 years)[a]	None	None	Bilateral cataracts (extracted at age 8 years, 15 years)	Bilateral cataracts (age ~12 years)	Normal	None	Normal
Nose	Unknown	Depressed nasal bridge; Anteverted nares	Depressed nasal bridge	Depressed nasal bridge	Depressed nasal bridge; Anteverted nares	Depressed nasal bridge; Short nose; Thick alae nasi	Short, depressed nasal bridge; Anteverted nares	Concave nasal ridge; Depressed nasal bridge	Short, upturned
Immunologic Abnormalities	None	None	Not assessed; Parental report of recurrent infections	Low neutrophil count (2 months of age)	Transient hypogamma globulinemia, Recurrent infections; Poor pneumococcal antibody response	Hypogamma globulinemi; Recurrent infections; Poor pneumococc al antibody response	Normal	None	Normal

Development	Normal	Normal	Expressive language delay	Normal	Normal	Normal	Normal	Normal	Abnormal findings
Other	Similarly affected sibling with same variants	Decreased carrying angle of elbows	Glottic and subglottic stenosis requiring tracheostomy (eventually removed)	Left cryptorchidism; subglottic stenosis requiring tracheostomy at 2 months	Possible subglottic stenosis (asymptomatic); Mild osteopenia	None	Mild joint laxity in fingers; Mild limitation of full extension at elbows.	None	At age 30 y, weight 40.8 kg (-4.3SD) an height 130.8 cm (-6.2SD). Family history includes two maternal third cousins (12 y/o female, 10 y/o male) with clinical diagnosis of SPONASTRIME dysplasia. Consanguinity was denied.

Table S3. Subjects with clinical diagnosis of SPONASTRIME dysplasia but without Biallelic Variants in *TONSL*

Subject ID	9[1]	10[2]	11[3]	12
Sex	M	M	F	M
Age at last follow-up	5 y 9 m	15 y 7 m	14 y	15 y 1 m
Height (Z-score)	-5.6	-5.36	-6.4	-1.61
Weight (Z-score)	-0.19	-4.09	-3.8	-0.61
FOC (Z-score)	Not available	0.10	-2.6	0.42
Disproportionate Short Stature	Unknown	Yes	Yes	No
Birth Parameters				
Gestational Age	Unavailable	Full Term	39 weeks	Not Available
Length	Unavailable	48.26 cm	NA	Not Available
Weight	Unavailable	2807 g	-1.3	Not Available
FOC	Unavailable	Not Available	Not Available	Not Available
Clinical Features				
Dental	Short dental roots	Mandibular overbite and wide spaced teeth	Extensive dental caries	Misaligned
Facial Features	Midface hypoplasia; Bifrontal bossing, Prominent mandible	Prominent forehead; Midface hypoplasia; Mild prognanthism; Mildly coarsened facial appearance	Frontal bossing; Midface hypoplasia	Mild malar hypoplasia; Low-set ears
Eye	Bilateral subcapsular cataracts at age 11 years	Normal dilated examination; Bilateral epicanthal folds	Strabismus	Epicanthi
Nose	Depressed nasal bridge	Depressed nasal bridge; Anteverted nares	Saddle nose	Depressed and large nasal bridge
Immunologic	Hypogammaglobulinemia; Poor antibody response to tetanus and Haemophilus vaccinations	None known	Clinically normal	Clinically normal
Orthopedic	Mild genu valgum; Limitation in extension of elbows; Mild joint laxity	Bilateral genu valgum; Brachydactyly; Progressive kyphoscoliosis requiring T2-L4 posterior spinal fusion at age 11 years	No other issues	Scoliosis surgery
Development	Normal	Normal	Severe intellectual disability	Normal
Radiographic Features				
Metaphyses	Irregularities with striations	Mild metaphyseal irregularities; Metaphyseal striations evident at age 10 years.	Striations	Striations with sclerosis
Epiphyses	Epiphyseal abnormalities	Normal	Normal	Normal
Spine	Platyspondyly	Platyspondyly; Ovoid and biconcave vertebral shape,	Thoracic kyphosis; Increased lumbar lordosis indentation of	Biconvex vertebrae with reduced posterior vertical height, left

	Reduced height of vertebral bodies; Anterior portion of the vertebral body is taller than posterior portion with central anterior protuberance	hypoplastic dens without instability	vertebral endplates, thickened endplates, reduced height	thoracic scoliosis, surgically fused T4-L1 at age 12.
Other Skeletal Findings	Coxa vara	Short and wide femoral necks; J-shaped sella; Proximal pointing of the 3rd, 4th and 5th metacarpals; Mild osteopenia	Carpal ossification delay; Brachymetacarpia	Sclerotic zones in phalanges, metacarpal and metatarsal bone
Other		Mildly limited bilateral elbow extension; Hypernasal voice; Multiple otitis media requiring PE tubes; Juvenile polyp		

[1] Heterozygous variant in *TONSL* noted (NM_013432.4:c.2800C>T, p.(Arg934Trp), rs75557541) but no second variant detected. Patient was previously published[1,2].

[2] Heterozygous variant in *TONSL* noted (NM_013432.4:c.25+2dupT) but no second variant detected.

[3] Patient was previously published[3].

Table S4. Additional Subject Characteristics for Subjects without Clinical Diagnosis of SPONASTRIME Dysplasia

Subject ID	6	7-1	7-2	8
Diagnosis	Spondylometaphyseal Dysplasia	Spondylometaphyseal Dysplasia	Spondylometaphyseal Dysplasia	Spondylometaphyseal Dysplasia
Sex	F	F	M	F
Age at last follow-up	12 y	10 y 9 m	9 y 9 m	5 y 11 m
Birth Parameters				
Gestational Age	34 weeks	39 5/7 weeks	37 4/7 weeks	35 2/7 weeks
Length	-2.64	0.36	1.33	-2.54
Weight	-1.54	-0.34	-0.49	-1.91
FOC	-1.10	0.33	-0.47	-1.49
Extra-Skeletal Features				
Dental	Delayed tooth eruption, small teeth	Delayed tooth eruption; Tooth discoloration; High palate	Delayed tooth eruption; Tooth discoloration; Upper lateral incisor is malpositioned; High palate	Normal
Facial Features	High forehead, frontal bossing; Hypoplasia of supra-orbital ridges	Short philtrum	Poorly defined philtrum	Short philtrum
Eye	Acoria; Deep set eyes; Primary aphakia; Microphthalmia; Short palpebral fissures; Bilateral epicanthal folds; Glaucoma (bilateral) likely secondary to aphakia	Wears glasses	No known abnormalities	Epicanthal folds with mild synophrys
Nose	Broad and depressed nasal bridge with crease over the bridge; Anteverted nares	Bulbous tip	Broad and depressed and nasal bridge	Depressed nasal bridge
Immunologic Abnormalities	None	Hypogammaglobulinemia; Vaccine responses untested due to immunoglobulin replacement; Congenital neutropenia	Hypogammaglobulinemia; Vaccine responses untested due to immunogloblulin replacement;Congenital neutropenia; Frequent infections	Transient hypogammaglobulinemia of infancy; Low memory B cell percentages Congenital neutropenia with normocellular bone marrow with myeloid hypoplasia and left shift; Failure to respond to the polysaccharide-restricted serotypes in the 23-valent pneumococcal vaccine; Recurrent infections
Development	Normal; Vision impairment impacts her motor performance	Normal	Normal	Mild global delay, now resolved

Other	Osteopenia; Low set ears; High-arched palate	Brittle toe nails	Growth hormone deficiency via glucagon stimulation test; Absence seizures; Dystrophic toenails	Asymmetric renal length; Multiple otitis media requiring PE tubes

Supplemental References:

1. Gripp, K.W. *et al.* Expanding the phenotype of SPONASTRIME dysplasia to include short dental roots, hypogammaglobulinemia, and cataracts. *Am J Med Genet A* **146A**, 468-73 (2008).
2. Langer, L.O., Jr., Beals, R.K., LaFranchi, S., Scott, C.I., Jr. & Sockalosky, J.J. Sponastrime dysplasia: five new cases and review of nine previously published cases. *Am J Med Genet* **63**, 20-7 (1996).
3. Camera, G., Camera, A., Di Rocco, M. & Gatti, R. Sponastrime dysplasia: report on two siblings with metal retardation. *Pediatr Radiol* **23**, 611-4 (1993).

Table S5. Exome Coverage Statistics and Number of Rare or Novel Variants Identified and Analyzed in the Exomes

Individual ID	1	2	3	4	5	6	7-1	7-2	8	9	10	11	12	13	14	15
Exome coverage	143X	117X	75X	Sanger only	99X	NA	159x	137x	118x	97X	45X	83X	114X	141X	44X	Sanger only
% coding regions covered at 10x	97%	95%	95%		88% at 15X	NA	98%	98%	96%	91%	98% at 8X	94%	98%	97%	89%	
% coding regions covered at 20x	96%	92%	90%		82% at 30X	NA	97%	97%	95%	87%	89%	90%	97%	97%	73%	
Rare or novel variants (SNVs and indels)	782	997	433		342	641	697	677	438	716	271	861	525	484	274	
Rare or novel variants in known skeletal dysplasia genes	9	14	3		NA	NA	4	4	9	11	NA	8	9	8	NA	
Rare or novel variants in genes explaining the phenotype	0	0	0		0	0	0	0	0	0	0	0	0	0	0	

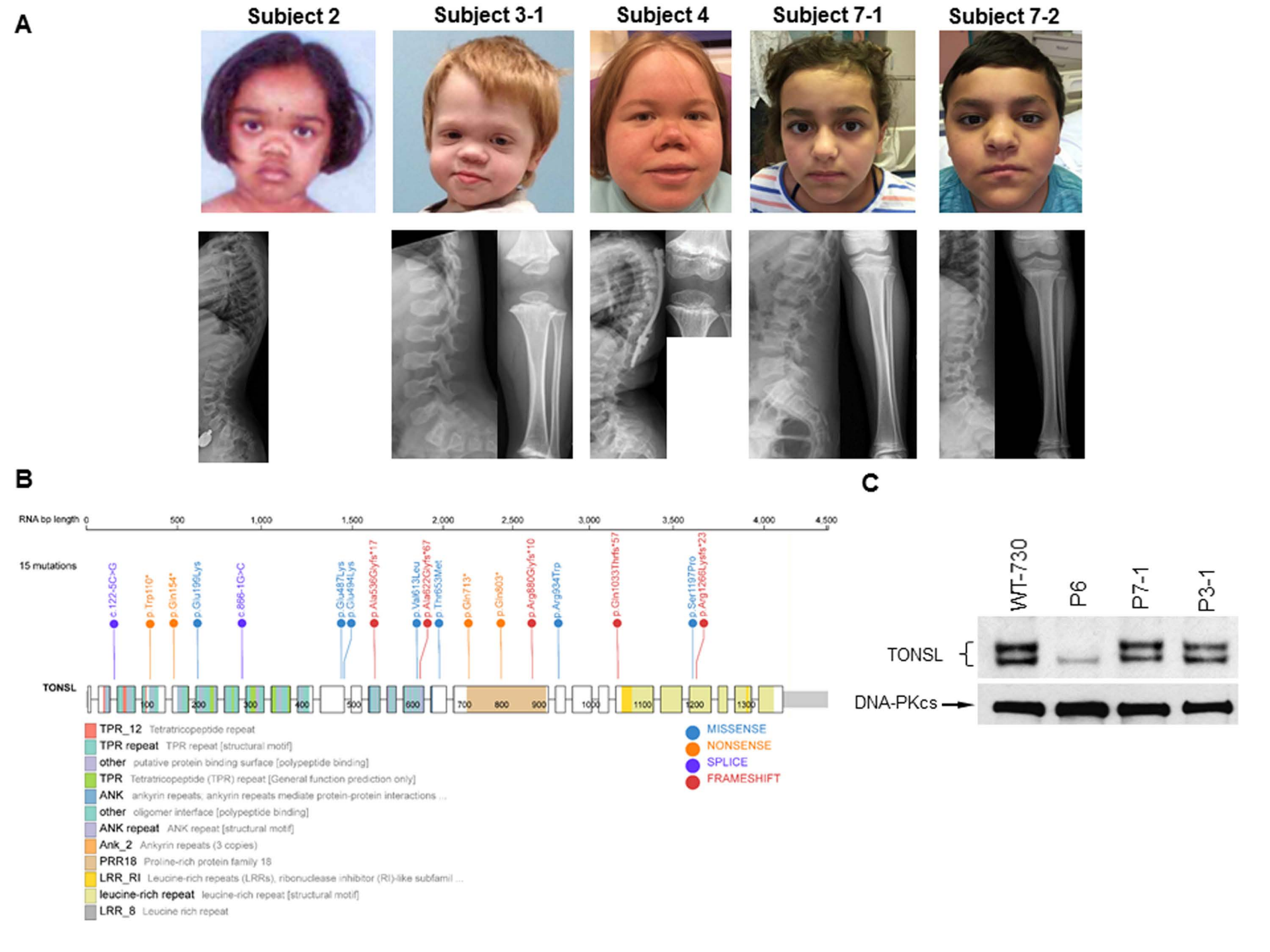
A
Subject 2
Subject 3-1
Subject 4
Subject 7-1
Subject 7-2
B
RNA bp length
15 mutations
c.122-5C>G
p.Trp110*
p.Gln154*
p.Glu196Lys
c.866-1G>C
p.Glu487Lys
p.Glu494Lys
p.Ala536Glyfs*17
p.Val613Leu
p.Ala522Glyfs*67
p.Thr653Met
p.Gln713*
p.Gln803*
p.Arg880Glyfs*10
p.Arg934Trp
p.Gln1033Thrfs*57
p.Ser1197Pro
p.Arg1266Lysfs*23
TONSL
TPR_12 Tetratricopeptide repeat
TPR repeat TPR repeat [structural motif]
other putative protein binding surface [polypeptide binding]
TPR Tetratricopeptide (TPR) repeat [General function prediction only]
ANK ankyrin repeats, ankyrin repeats mediate protein-protein interactions ...
other oligomer interface [polypeptide binding]
ANK repeat ANK repeat [structural motif]
Ank_2 Ankyrin repeats (3 copies)
PRR18 Proline-rich protein family 18
LRR_RI Leucine-rich repeats (LRRs), ribonuclease inhibitor (RI)-like subfamil ...
leucine-rich repeat leucine-rich repeat [structural motif]
LRR_8 Leucine rich repeat
MISSENSE
NONSENSE
SPLICE
FRAMESHIFT
C
WT-730
P6
P7-1
P3-1
TONSL
DNA-PKcs

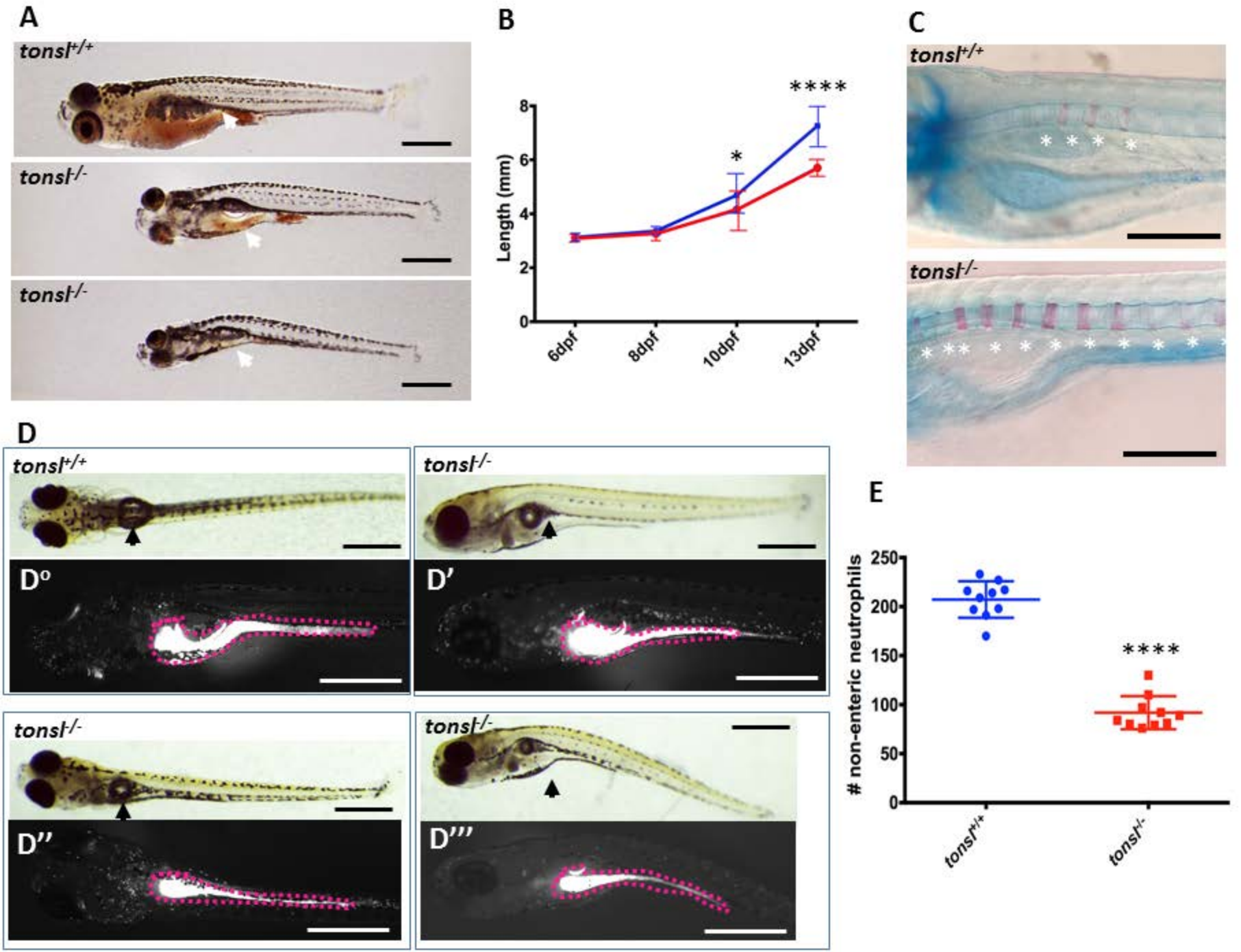
A
tonsl+/+
tonsl-/-
tonsl-/-
B
Length (mm)
8
6
4
2
0
6dpf
8dpf
10dpf
13dpf
*
****
C
tonsl+/+
tonsl-/-
D
tonsl+/+
tonsl-/-
Do
D'
tonsl-/-
tonsl-/-
D''
D'''
E
non-enteric neutrophils
250
200
150
100
50
0
****
tonsl+/+
tonsl-/-

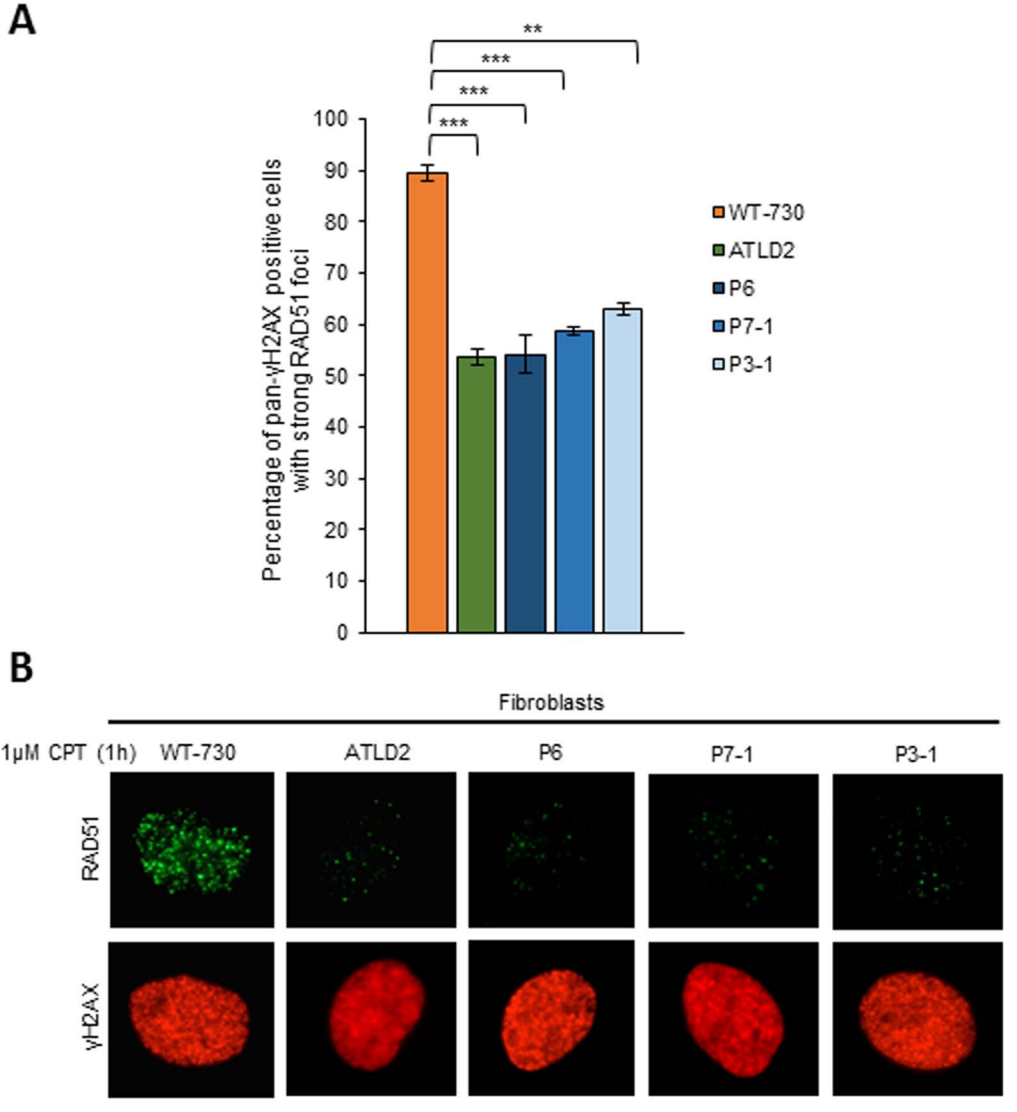
A
**
***
***
***
100
90
80
70
60
50
40
30
20
10
0
Percentage of pan-γH2AX positive cells with strong RAD51 foci
WT-730
ATLD2
P6
P7-1
P3-1
B
Fibroblasts
1μM CPT (1h)
WT-730
ATLD2
P6
P7-1
P3-1
RAD51
γH2AX

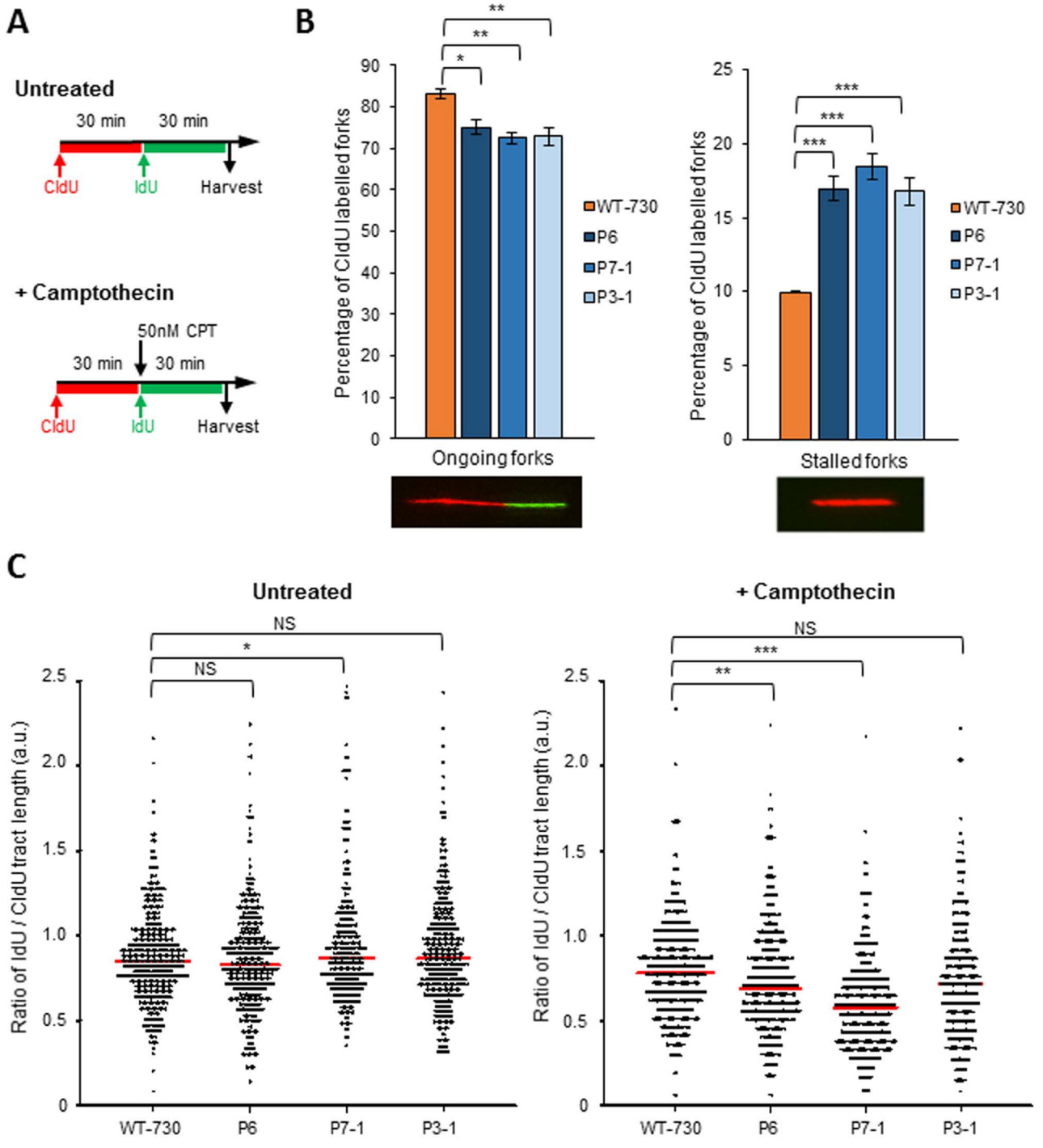
A
Untreated
30 min
30 min
CldU
IdU
Harvest
+ Camptothecin
50nM CPT
30 min
30 min
CldU
IdU
Harvest
B
Percentage of CldU labelled forks
Ongoing forks
Stalled forks
WT-730
P6
P7-1
P3-1
C
Untreated
+ Camptothecin
Ratio of IdU / CldU tract length (a.u.)
NS
*
**
***
WT-730
P6
P7-1
P3-1

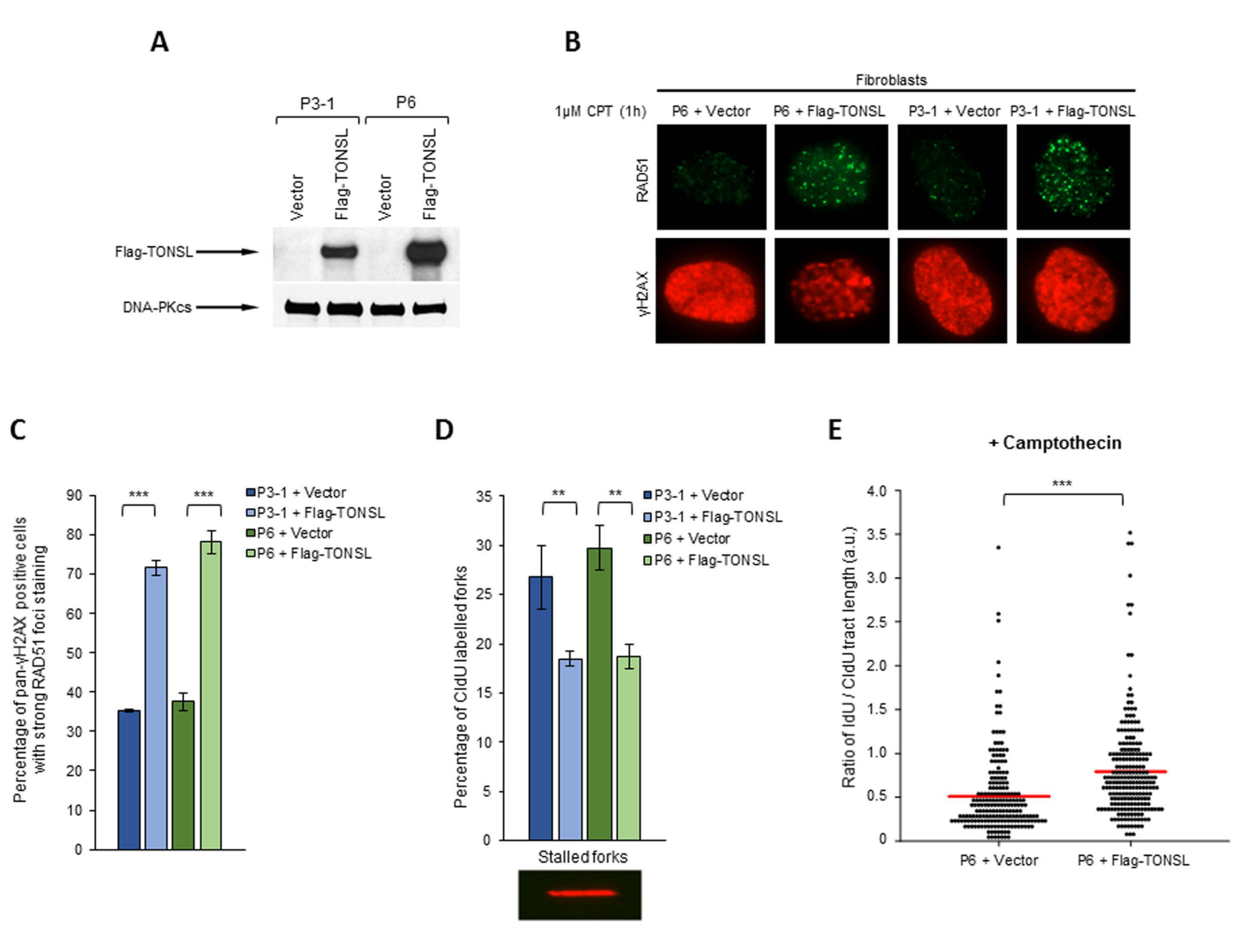
A
P3-1
P6
Vector
Flag-TONSL
Vector
Flag-TONSL
Flag-TONSL
DNA-PKcs
B
Fibroblasts
1μM CPT (1h)
P6 + Vector
P6 + Flag-TONSL
P3-1 + Vector
P3-1 + Flag-TONSL
RAD51
γH2AX
C
Percentage of pan-γH2AX positive cells with strong RAD51 foci staining
***
***
P3-1 + Vector
P3-1 + Flag-TONSL
P6 + Vector
P6 + Flag-TONSL
D
Percentage of CldU labelled forks
**
**
P3-1 + Vector
P3-1 + Flag-TONSL
P6 + Vector
P6 + Flag-TONSL
Stalled forks
E
+ Camptothecin
***
Ratio of IdU / CldU tract length (a.u.)
P6 + Vector
P6 + Flag-TONSL

A

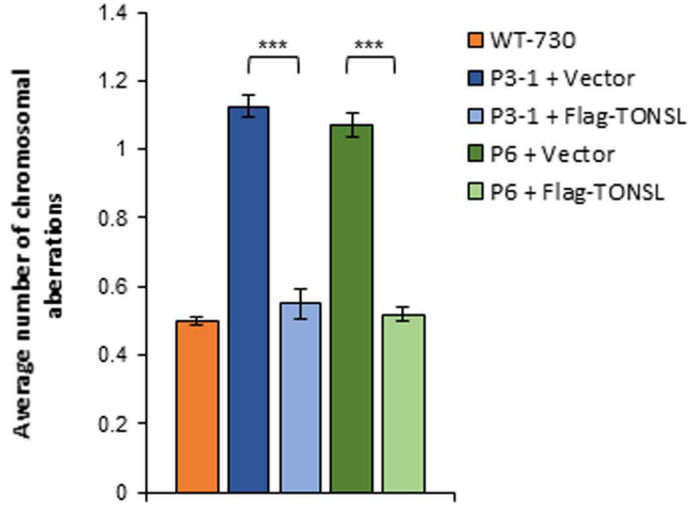
Average number of chromosomal aberrations
1.4
1.2
1
0.8
0.6
0.4
0.2
0
***
***
WT-730
P3-1 + Vector
P3-1 + Flag-TONSL
P6 + Vector
P6 + Flag-TONSL

B

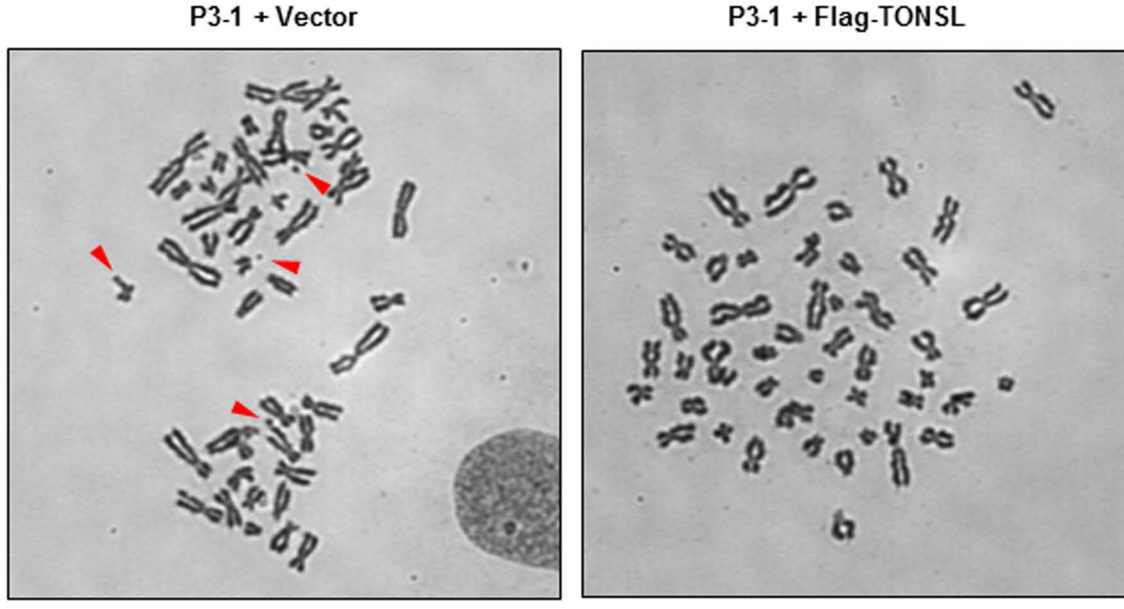
P3-1 + Vector
P3-1 + Flag-TONSL

Figure S1. Additional photographs. (A) Subject 2 at 6 years of age showing rhizomelia, mesomelia and genu valgum. (B) Subject 4 at 22 years of age. Additional radiographs and photographs have been published previously (8). (C) Subject 6 at 12 years of age. (D) Twisted lateral incisors observed in subject 4 (bilateral). (E) Twisted lateral incisor observed in subject 7-2 (unilateral).

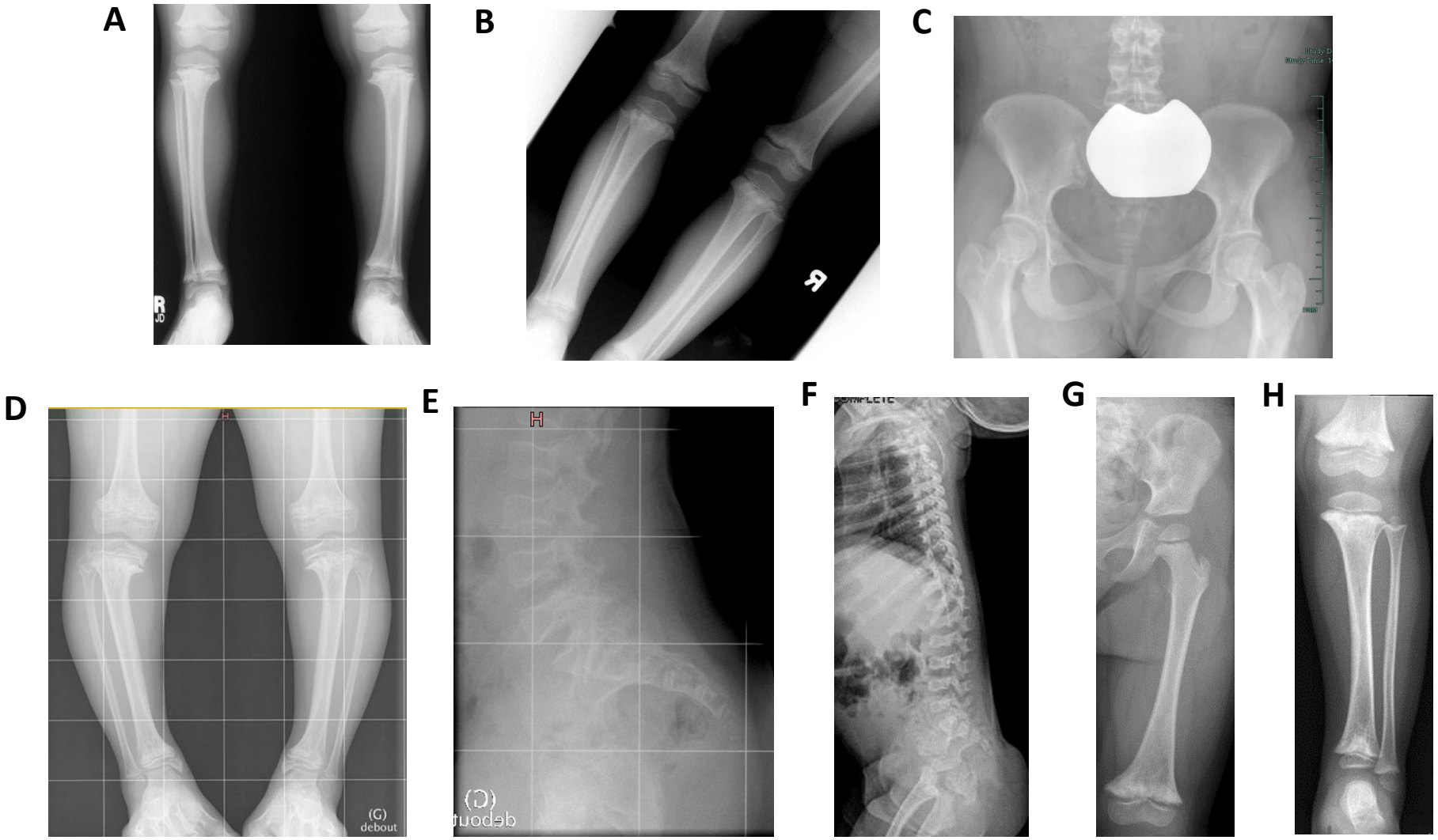

Figure S2. Additional radiographs. (A) Subject 1, 6 years 8 months. Metaphyseal widening and irregularities are apparent in tibia. (B) Subject 1, childhood, age unknown. Metaphyseal striations and irregularities are apparent in tibia and femur. (C) Subject 1, 13 years, 3 month. Femoral necks appear short and wide. (D) Subject 5, 11 years. Metaphyseal striations and irregularities are noted in tibia and femur with varus bowing. (E) Subject 5, 11 years. Platyspondyly and biconcave vertebrae are noted. (F) Subject 8, 1 year 5 months. Platyspondyly noted. Several of the vertebral bodies also have a biconcave shape. Note the distinct junction between anterior and posterior portions of the lumbar vertebral bodies. (G) Subject 8, 4 years 5 months. Widening, sclerosis, and irregularity and mild striations of the distal femoral metaphysis are noted. (H) Subject 8, 4 years 5 months. Widening, sclerosis, and irregularity and mild striations of the proximal tibial metaphysis are noted.

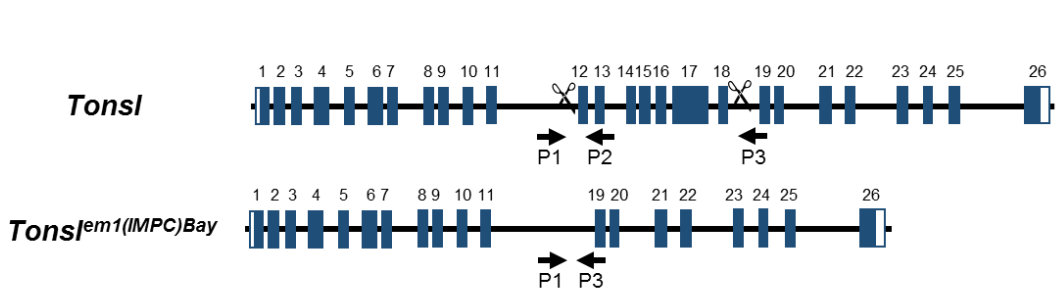

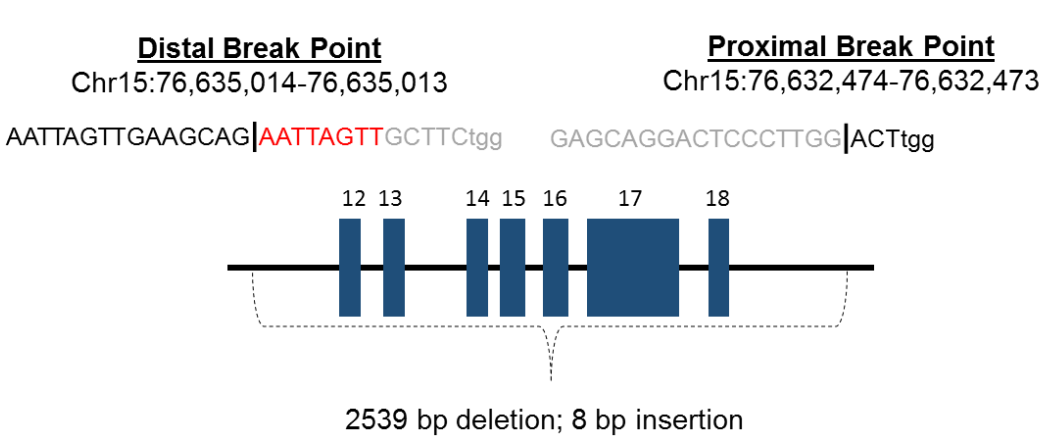

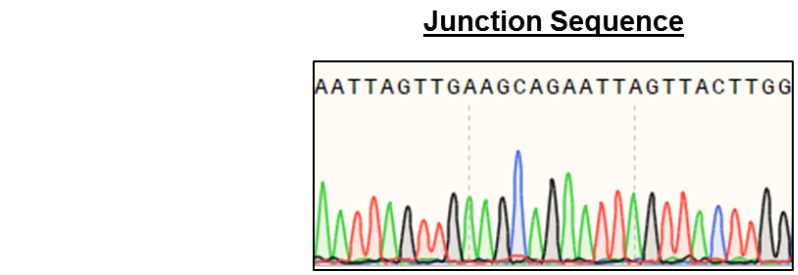

Figure S3. *Tonsl deletion analysis.* (A) Schematic representation of the *Tonsl* locus. The exon/intron structure of the wild-type and null (*Tonsl*$^{em1(IMPC)Bay}$) allele are shown. Exons 12-18 are deleted in the null allele. Blue boxes = coding sequence; White boxes = UTRs. Scissors represent sgRNA target sites. Arrows indicate primers P1, P2, and P3 used for genotyping and sequencing (P1 and P2 amplify the wild-type allele; P1 and P3 amplify the null allele). (B) Distal (Chr15:76,635,014-76,635,013; GRCm38/mm10) and proximal (Chr15:76,632,474-76,632,473; GRCm38/mm10) breakpoints of the deletion in *Tonsl*$^{em1(IMPC)Bay}$. *Tonsl* is oriented in the antisense direction in the mouse genome. Sequence text in black and gray are the sgRNA target and protospacer adjacent motif (PAM) sequences. Red sequence text is an 8 bp insertion that occurred during nonhomologous end joining (NHEJ). (C) Chromatogram showing DNA sequence of the nonhomologous end joining (NHEJ) repair junction.

tonsl^{b1347} c.234-8; p.E80G21Ter

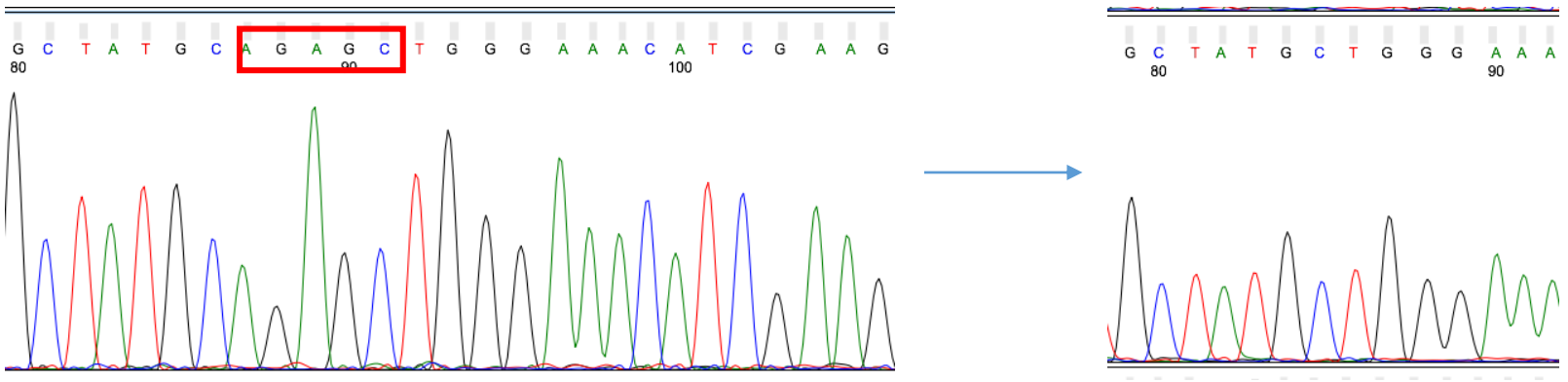

tonsl^{b1348} c.235-47; p. E80S4Ter

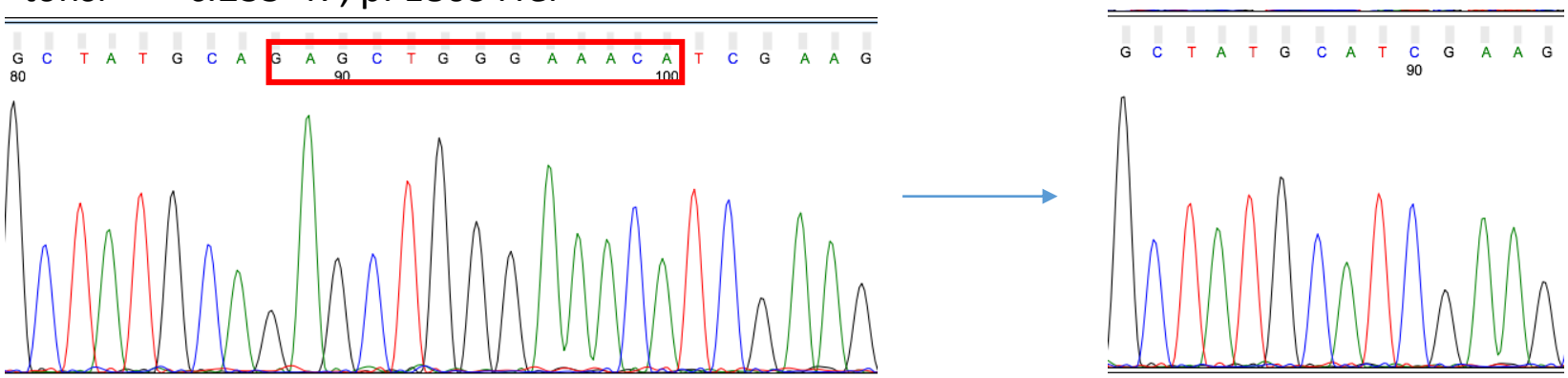

Figure S4. Zebrafish CRISPR mutants. Frameshift alleles of *tonsl* affect the two alternate reading frames of exon 3. Bases deleted in each allele are boxed in red; homozygous mutant sequence is presented on the left for each allele.